

Response to Reviewer/Editor

1

2

3 -The author agrees with the reviewer that Figure 4 is redundant given existence of other figures which
4 show study region, and was not worthy of a supplemental section. It has been removed from the paper.

5

6 -The reviewer correctly spotted a mistake in the written emission totals in the first sentence of the
7 discussion section. This has been fixed to match text elsewhere.

8

9 -An adjustment was made to the department of one of the co-authors.

10

11 -A sentence was added in the acknowledgement section to acknowledge the gratefulness of the author
12 for their hard work catching the many stupid and smart mistakes scattered throughout the paper.

13 Quantifying methane emissions from natural gas production in 14 northeastern Pennsylvania

15 Zachary R. Barkley¹, Thomas Lauvaux¹, Kenneth J. Davis¹, Aijun Deng¹, ~~Yanni Cao¹~~, Natasha L.
16 Miles¹, Scott J. Richardson¹, ~~Yanni Cao²~~, Colm Sweeney²~~Sweeney³~~, Anna Karion³~~Karion⁴~~, MacKenzie
17 Smith⁴~~Smith⁵~~, Eric A. Kort⁴~~Kort⁶~~, Stefan Schwietzke⁵~~Schwietzke⁶~~, Thomas Murphy⁶~~Murphy⁷~~, Guido
18 Cervone⁷~~Cervone⁸~~, Douglas Martins⁸~~Martins⁹~~, Joannes D. Maasakkers⁹~~Maasakkers¹⁰~~

19 ¹Department of Meteorology, The Pennsylvania State University, University Park, PA 16802, United States

20 ²~~NOAA²Department of Geography, The Pennsylvania State University, University Park, PA 16802, United States~~

21 ³NOAA/Earth Systems Research Laboratory, University of Colorado, Boulder, CO, 80305, United States

22 ³~~National⁴National~~ Institute of Standards and Technology, Gaithersburg, MD 20899, United States

23 ⁴~~Department⁵Department~~ of Climate and Space Sciences and Engineering, University of Michigan, Ann Arbor, MI, 48109,
24 United States

25 ⁵~~Cooperative⁶Cooperative~~ Institute for Research in Environmental Sciences, University of Colorado, Boulder, Colorado,
26 USA.

27 ⁶~~Marcellus⁷Marcellus~~ Center for Outreach and Research, The Pennsylvania State University, University Park, PA 16802,
28 United States

29 ⁷~~Department⁸Department~~ of Geography, The Pennsylvania State University, University Park, PA 16802, United States

30 ⁸FLIR⁹FLIR Systems, West Lafayette, IN 47906, United States

31 ⁹~~School¹⁰School~~ of Engineering and Applied Sciences, Harvard University, Pierce Hall, 29 Oxford Street, Cambridge,
32 Massachusetts 02138, United States

33

34

35 *Correspondence to:* Zachary R. Barkley (zrb5027@psu.edu)

36

37

38 **Abstract.** Natural gas infrastructure releases methane (CH₄), a potent greenhouse gas, into the atmosphere. The estimated
39 emission rate associated with the production and transportation of natural gas is uncertain, hindering our understanding of its
40 greenhouse footprint. This study presents a new application of inverse methodology for estimating regional emission rates
41 from natural gas production and gathering facilities in northeastern Pennsylvania. An inventory of CH₄ emissions was
42 compiled for major sources in Pennsylvania. This inventory served as input emission data for the Weather Research and
43 Forecasting model with chemistry enabled (WRF-Chem), and atmospheric CH₄ mole fraction fields were generated at 3 km
44 resolution. Simulated atmospheric CH₄ enhancements from WRF-Chem were compared to observations obtained from a
45 three-week flight campaign in May 2015. Modelled enhancements from sources not associated with upstream natural gas
46 processes were assumed constant and known and therefore removed from the optimization procedure, creating a set of
47 observed enhancements from natural gas only. Simulated emission rates from unconventional production were then adjusted
48 to minimize the mismatch between aircraft observations and model-simulated mole fractions for ten flights. To evaluate the
49 method, an aircraft mass balance calculation was performed for four flights where conditions permitted its use. Using the
50 model optimization approach, the weighted mean emission rate from unconventional natural gas production and gathering

51 facilities in northeastern Pennsylvania approach is found to be 0.36% of total gas production, with a 2σ confidence interval
52 between 0.27-0.45% of production. Similarly, the mean emission estimates using the aircraft mass balance approach is
53 calculated to be 0.40% of regional natural gas production, with a 2σ confidence interval between 0.08-0.72% of production.
54 These emission rates as a percent of production are lower than rates found in any other basin using a top-down methodology,
55 and may be indicative of some characteristics of the basin that makes sources from the northeastern Marcellus region unique.

56 **1 Introduction**

57 The advent of hydraulic fracturing and horizontal drilling technology has opened up the potential to access vast reservoirs of
58 natural gas previously inaccessible, shifting energy trends in the United States away from coal and towards natural gas (EIA,
59 2016b). From a greenhouse gas (GHG) emissions perspective, natural gas has the potential to be a cleaner energy source
60 than coal. For every unit of energy produced, half as much carbon dioxide (CO_2) is emitted through the stationary
61 combustion of natural gas in comparison to coal (EPA, 2016). However, during the process of extracting and distributing
62 natural gas a percentage of the overall production escapes into the atmosphere through both planned releases and unintended
63 leaks in infrastructure. Though these emissions may be small from an economic perspective, their climatological impacts are
64 not negligible (Alvarez et al., 2012; Schwietzke et al., 2014). Methane (CH_4), the main component of natural gas, is a potent
65 greenhouse gas with a global warming potential over a 20-year period (GWP_{20}) of 84 (Myhre et al., 2013). Over a 100-year
66 period the GWP is reduced to 28 due mostly to interactions with the hydroxyl radical which transform the CH_4 molecule to
67 CO_2 . Depending on which timespan is used, the relative climatological impacts of natural gas as an energy source compared
68 to coal can vary. Using the GWP_{20} value, it is estimated that a natural gas emission rate of greater than 3% of total gas
69 production would result in a natural gas power plant having a more negative impact on the climate than a coal-powered
70 plant. Using the GWP_{100} value, this emission rate threshold shifts to 10% of production (Schwietzke et al., 2014; Alvarez et
71 al., 2012). Complicating matters further, the future climate impacts associated with an increased availability of natural gas
72 extends well beyond a simple greenhouse gas footprint comparison against coal. Lower fuel prices linked to this new
73 reservoir of energy can change the course of future energy development globally. With many states and countries attempting
74 to find a suitable balance between their energy policies and greenhouse gas footprint, it is important for the scientific
75 community to be able to quantify and monitor natural gas emission rates.

76 The drilling and transportation of natural gas can be broken down into five stages: production, processing, storage,
77 transmission, and distribution. The United States Environmental Protection Agency (EPA) uses a bottom-up approach to
78 quantify these emissions, estimating emission rates per facility or component (such as a compressor, unit length of pipeline,
79 pneumatic device) or an average emission per event (such as a well completion or liquids unloading). These “emission
80 factors” are then multiplied by nationwide activity data containing the number of components or events associated with each
81 emission factor, and a total emission rate is produced for the country (EPA, 2015b). This bottom-up approach is a practical
82 methodology for estimating emissions over a large scale but has limitations. A bottom-up inventory depends on the quality

83 and quantity of its emission factors and activity data. Emissions from sources in the natural gas industry can be temporally
84 variable and have a wide range of values depending on a number of factors, such as the quality and age of the device and the
85 gas pressure moving through the component. Furthermore, recent studies have shown that a majority of emissions comes
86 from a small percentage of devices, often referred to as “super-emitters”, creating a long-tail distribution of emission sources
87 (Brandt et al., 2014, Omara et al., 2016, Zavala-Araiza et al., 2015, 2017, Frankenberg et al., 2016). These factors make it
88 difficult to sample enough devices and adequately describe the mean emission rate, thus allowing for significant
89 representation errors in the emission factors. Because emission factors are required for hundreds of different components,
90 these errors can accumulate and lead to systematic biases in the total emissions estimate.

91 One way to compliment results based on inadequate sample sizes in the bottom-up approach is to measure the
92 aggregated enhancement in the atmospheric mole fraction at larger scales through a top-down approach. Instead of
93 measuring emissions from individual devices and scaling up, a top-down approach takes atmospheric greenhouse gas
94 concentrations measured downwind of a continent (e.g. Bousquet et al., 2006), a region (e.g. Lauvaux et al., 2008), a city
95 (e.g. White et al., 1976, Mays et al., 2009, Lamb et al., 2016) or a facility (e.g. Ryerson et al., 2001) and uses inverse
96 methodologies to attribute the enhancements to potential sources upwind. One of these methods, the aircraft mass balance
97 technique, has been performed at many different oil and gas fields to characterize natural gas emissions (Petron et al., 2012,
98 Karion et al., 2013, 2015, Peischl et al., 2015, Conley et al., 2016). While this methodology is able to capture surface fluxes
99 over a large region, it remains difficult to attribute the emissions to any individual source (Cambaliza et al., 2014). Any
100 sources from within the flux region that emit CH₄ will be measured in the downwind observations and be a part of the
101 aggregated regional enhancement. Atmospheric observations may include other sources of CH₄ unrelated to natural gas, such
102 as anaerobic respiration from landfills and wetlands, enteric fermentation from cattle, anaerobic decomposition of manure,
103 CH₄ seepage from coal mining, and many other smaller sources. If the purpose of the study is to solve for the emissions from
104 the natural gas industry, emissions from all sources unrelated to natural gas must be known and removed from the regional
105 flux estimate. Thus, top-down experiments require an accurate CH₄ inventory of the study area and any errors associated
106 with the inventory will propagate into the final emissions estimate. A more advanced technique to separate out non-natural
107 gas sources has been developed using ethane as a tracer for natural gas (Smith et al., 2015). However, such methods may
108 struggle in dry gas basins where smaller ethane to methane ratios within the gas can make the ethane signature more difficult
109 to separate out, or in regions where multiple ethane sources are present. And similar to bottom-up methods, top-down studies
110 fail to address temporal variability, with observations from many of these studies having been collected during a limited
111 number of 2 to 4 hour aircraft flights performed over a period of weeks.

112 In recent years, both bottom-up and top-down studies have aimed at calculating natural gas emission rates, with
113 bottom-up studies generally finding smaller emission rates than their top-down counterparts (Brandt et al., 2014). The
114 discrepancy between the results from these two methodologies must be better understood if the true emission rate is to be
115 known. Both the bottom-up and top-down approaches have their own inherent sources of error. For the bottom-up approach,
116 a small sample size could result in the omission of any super-emitters, resulting in a low emissions bias. For the top-down

117 approach, difficulty in attributing the measured enhancements to their correct sources can lead to errors when solving for the
118 emissions of a particular sector.

119 Top-down emission estimates of individual basins have shown variation in the emission rate across the different
120 basins. An aircraft mass balance performed over the Barnett shale in Texas found an emission rate between 1.3-1.9% of
121 production (Karion et al., 2015), yet a similar mass balance study executed over unconventional wells in Uintah County,
122 Utah, calculated an emission rate between 6.2-11.7% of production (Karion et al., 2013). Differences in regional emission
123 rates can perhaps best be illustrated by recent studies in the Marcellus region. The Marcellus shale gas play is part of the
124 Marcellus geological formation running close to the Appalachian mountain chain from West Virginia to southern New York
125 and contains an estimated 140 billion cubic feet of technically recoverable natural gas (EIA, 2012). Reaching peak
126 production by the end of 2015, the Marcellus is the largest producing shale in the U.S., producing 17,000 million standard
127 cubic feet per day (MMSCFD) of natural gas (EIA, 2016a). A bottom-up study measuring emissions from 17 unconventional
128 well-sites in the Marcellus found a median emission rate from the wells of 0.13% of production, but estimated a mean
129 emission rate between 0.38-0.86% of production due to the potential presence of super-emitters which would skew the mean
130 emission rate towards values higher than the median (Omara et al., 2016). An aircraft mass balance study over northeastern
131 Pennsylvania calculated an emission rate between 0.18-0.41%, a number that accounted for emissions from the production,
132 processing, and transmission of the gas (Peischl et al., 2015). Both of these derived estimates fall below emission rates
133 calculated throughout other basins and are below the 3% threshold required for natural gas to be a smaller climate pollutant
134 in comparison to coal over a 20-year timescale. The low rates in the Marcellus compared to other regions could be the result
135 of a systematic difference within the Marcellus that leads to a more efficient extraction of natural gas. However, while useful
136 as a first-guess estimation, current studies performed in the region are based on relatively small sample sizes (1 aircraft mass
137 balance and 88 individual well measurements). A more thorough analysis of the emission rate in the Marcellus would
138 provide insight into regional differences in CH₄ emissions from different shale basins and help improve national estimates of
139 emissions from natural gas.

140 This study seeks to provide confidence in the emission rate for the northeastern Marcellus by performing the most
141 thorough top-down analysis of the northeastern Marcellus region to date. CH₄ measurements were taken from aircraft
142 observations across 10 flights in northeastern Pennsylvania. A new implementation of modelling CH₄ mole fractions is
143 developed to track complex plume structures associated with different emitters, and an optimal natural gas emission rate is
144 solved for each of the 10 flights. An aircraft mass balance technique is also conducted for 4 of the flights and natural gas
145 emission estimates from this method are compared to those calculated using the modelling technique. Using information on
146 the uncertainty with both methods, a regional emission rate is calculated for the natural gas industry in the northeastern
147 Marcellus region.

148 **2 Methods**

149 The objective of this study is to quantify CH₄ emissions coming from unconventional wells and compressor stations,
150 henceforth referred to as upstream natural gas emissions, in the northeastern Marcellus region (defined as the area contain
151 within 41.1-42.2°N 75.2-77.6°W, see Figure 1) through two different top-down methodologies. CH₄ observations from
152 aircraft data are collected for ten (10) individual flights over a three-week period in May 2015. These data are used to solve
153 for the upstream natural gas emission rate using an aircraft mass balance approach. Additionally, a CH₄ emissions inventory
154 for the region is compiled and input into an atmospheric transport model described below. CH₄ concentrations are modelled
155 for each flight, and the upstream natural gas emission rate within the model is optimized to create the best match between
156 aircraft observations and model projected enhancement, providing another estimate for the upstream natural gas emission
157 rate. The sections below detail the regional CH₄ inventory, the aircraft campaign, the transport model, the model
158 optimization technique, and the mass balance approach used in this study.

160 **2.1 Regional Methane Emission Inventory**

161 In this study we characterize emissions from the natural gas industry into five different sectors: emissions from wells,
162 emissions from compressor facilities, emissions from storage facilities, emissions from pipelines, and emissions in the
163 distribution sector.

164 To estimate CH₄ emissions from the production sector of the natural gas industry, data were first obtained on the
165 location and production rate of each unconventional well from the Pennsylvania Department of Environmental Protection
166 Oil and Gas Reporting website (PADEP, 2016) and the West Virginia Department of Environmental Protection (WVDEP,
167 2016). To convert the production rate into an emission rate, we need to assume a first-guess as to the expected leakage from
168 wells in the area. A first-guess natural gas emission rate of 0.13% was applied to the production value of each of the 7000+
169 producing unconventional wells based on the median rate from Omara et al., (2016). The natural gas emission rate was then
170 converted to a CH₄ emission rate by assuming a CH₄ composition in the natural gas of 95% (Peischl et al., 2015).

171 In addition to unconventional wells, the domain also contains more than 100,000 shallow conventional wells.
172 Annual conventional production rates for the year 2014 were obtained through the PADEP Oil and Gas Reporting website,
173 the WVDEP, and the New York Department of Environmental Conservation (NYDEC, 2016). Despite the large number of
174 wells, the average conventional well in PA produces 1% of the natural gas compared to its unconventional counterpart.
175 However, it is speculated that the older age of these wells and a lack of maintenance and care for them results in a higher
176 emission rate for these wells as a function of their production (Omara et al., 2016). A first-guess natural gas emission rate of
177 11% was applied to the production values of the conventional wells based on the median emission rate from the wells
178 sampled in Omara et al., (2016). Similar to the unconventional wells, the natural gas emission rate was then converted to a
179 CH₄ emission rate by assuming a CH₄ composition in the natural gas of 95%.

180 Compressor stations located within the basin are responsible for collecting natural gas from multiple well locations,
181 removing non-CH₄ hydrocarbons and other liquids from the flow, and regulating pressure to keep gas flowing along
182 gathering and transmission pipelines, and can be a potential source for methane emissions. Data for compressor station
183 locations and emissions comes from a dataset used in Marchese et al., (2015). A total of 489 compressor facilities are listed
184 for Pennsylvania, with 87% of the listed facilities also containing location data. Emissions for each compressor station are
185 calculated through two different methodologies. In the simplest case, a flat emission rate of 32.35 kg hr⁻¹ is applied for each
186 station, the mean emission rate of a gathering facility in PA found in Marchese et al., (2015). In the more complex scenario,
187 the same emissions total is used as in the flat rate case, but is distributed among the compressor stations linearly as a function
188 of their energy usage. Wattage between compressors in our dataset can vary greatly, from 10 kW for small compressors to
189 7000 kW or more at large gathering facilities. Using the wattage as a proxy for emissions allows us to account for the size
190 and throughput of natural gas at each station and assumes larger stations will emit more natural gas compared to smaller
191 stations (Marchese et al., 2015).

192 Data on locations of underground storage facilities were obtained from the United States Energy Information
193 Administration (EIA, 2015). For each of these locations, a base emission rate of 96.7 kg hr⁻¹ was applied according to the
194 average value emitted by a compressor station associated with an underground storage facility (Zimmerle et al., 2016).

195 To calculate pipeline emissions, data on pipeline locations needed to be collected. Information on transmission
196 pipelines, which connect gathering compressors to distribution networks, is provided by the Natural Gas Pipelines GIS
197 product purchased from Platts, a private organization which collects and creates various infrastructural layers for the natural
198 gas and oil industry (Platts, 2016). Gathering pipeline data, corresponding to the transfer of gas from wellheads to gathering
199 compressors, is nearly non-existent for PA with the exception of Bradford County, which maps out all gathering pipeline
200 infrastructure within the county border. In PA, information on the location of a gathering pipeline elsewhere is only available
201 where a gathering line crosses a stream or river. To account for gathering pipelines in the remainder of the state, a GIS model
202 was created using Bradford County pipelines map in addition to previously generated pipeline maps of Lycoming County
203 (Langlois et al., 2017) as a typical pattern to simulate connecting pipelines between unconventional wells throughout the
204 state (Figure 2). The resulting pattern follows the valley of the Appalachian Mountains, with larger pipelines crossing
205 through the state to connect the different branches of the network. These pipelines were then multiplied by an emission
206 factor of 0.043 kg per mile of pipe, the factor used for gathering pipeline leaks in the Inventory of U.S. Greenhouse Gas
207 Emissions and Sinks: 1990-2013 (EPA, 2015b).

208 CH₄ emissions from natural gas distribution sources, coal mines, and animal/animal waste were provided from
209 Maasackers et al., (2016), which takes national scale emissions from the EPA's greenhouse gas inventory for the year 2012
210 and transforms it into a 0.1° × 0.1° emissions map for the continental U.S. For natural gas distribution emissions, various
211 pipeline data was collected at a state-level and emission factors were accounted for to calculate a total distribution emission
212 for the state. This emissions total was then distributed within the state proportional to the population density. Emission
213 estimates for coal are calculated using information from the Greenhouse Gas Reporting Program (GHGRP) for active mines

214 and the Abandoned Coal Mine Methane Opportunities Database for abandoned mines (EPA, 2008). State-level emissions
215 missions from enteric fermentation and manure management are provided in the EPA's inventory. These emissions were
216 segregated into higher resolutions using county-level data from the 2012 U.S. Census of Agriculture (USDA, 2012) and
217 land-type mapping.

218 Finally, the EPA's Greenhouse Gas Reporting Program dataset for the year 2014 was used to capture all other major
219 sources of CH₄ in the region otherwise unaccounted for, the majority of which are emissions from landfills and some
220 industrial sources (EPA, 2015a). Sources within the GHGRP that overlap with natural gas sources already accounted for
221 within our inventory were removed to prevent redundancy.

222 Although our emissions map used for the model runs did not account for potential CH₄ emissions from wetland
223 sources, a series of wetlands emission scenarios was obtained for the region using data from Bloom, et al., (2017). From this
224 dataset, wetland CH₄ emissions make up only 1% of all regional CH₄ emissions in the most extreme scenario, and thus we
225 assume their impact is negligible to this study.

226

227 **2.2 Aircraft Campaign**

228 Observations for this project were obtained from a 3-week aircraft campaign during the period of May 14th-June 3rd, 2015
229 and are available for public access (<https://doi.org/10.15138/G35K54>). The campaign was led by the Global Monitoring
230 Division (GMD) of the National Oceanic and Atmospheric Administration Earth Systems Research and Laboratory (NOAA
231 ESRL), in collaboration with the University of Michigan. During this period, the NOAA Twin Otter aircraft flew throughout
232 the northeast portion of Pennsylvania, providing a total of ten flights across nine days. The aircraft was equipped with a
233 Cavity Ring-Down Spectroscopic analyser (Picarro G2401-m) measuring CH₄, CO₂, CO, and water vapour mole fractions at
234 approximately 0.5Hz with a random error of 1 ppb, 0.1 ppm, 4 ppb, and 50 ppm respectively (Karion et al., 2013). GPS
235 location, horizontal winds, temperature, humidity, and pressure were also recorded at 1 Hz. The majority of observations for
236 each flight occurred during the afternoon hours at heights lower than 1500 m above ground level. Each flight contains at
237 least one vertical profile within and above the boundary layer, with temperature and water vapour observations from these
238 profiles used to estimate the atmospheric boundary layer height and ensure that the aircraft sampled air within the boundary
239 layer throughout the flight. Observations suspected of being located above the boundary layer top are flagged and removed
240 from all calculations.

241 Flight paths, wind speeds, and CH₄ observations for each of the 10 flights can be seen in Figure 3. For six of the ten
242 flights, a box pattern was flown around a large portion of unconventional natural gas wells in northeastern PA. These flights
243 were performed typically on days with a strong, steady wind, with a clearly defined upwind and downwind transect intended
244 for use in an aircraft mass balance calculation. Five of the six box-pattern flights were composed of two loops circling the
245 gas basin, allowing for two separate calculations of the upstream natural gas emission rate for the flight. On the remaining

246 four flights, raster patterns were performed to help identify spatial complexities of CH₄ emissions within the basin. All ten
247 flights were used in the model optimization calculation of the upstream natural gas emission rate.

248 **2.3 Transport Model**

249 The atmospheric transport model used in this study is the Advanced Weather Research and Forecasting (WRF) model
250 (WRF-ARW, Skamarock et al., 2008) version 3.6.1. The WRF configuration for the model physics used in this research
251 includes the use of: 1) the double-moment scheme (Thompson et al., 2004) for cloud microphysical processes, 2) the Kain-
252 Fritsch scheme (Kain and Fritsch 1990, Kain 2004) for cumulus parameterization on the 9-km grid, 3) the Rapid Radiative
253 Transfer Method for general circulation models (GCMs) (RRTMG, Mlawer et al., 1997, Iacono et al., 2008), 4) the level 2.5
254 TKE-predicting MYNN planetary boundary layer (PBL) scheme (Nakanishi and Niino 2006), and 5) the Noah 4-layer land-
255 surface model (LSM) that predicts soil temperature and moisture (Chen and Dudhia 2001, Tewari et al., 2004) in addition to
256 sensible and latent heat fluxes between the land surface and atmosphere.

257 | The WRF model grid configuration used in this research contains two grids: 9- and 3-km ~~(Figure 4)~~, each with a
258 mesh of 202x202 grid points. The 9-km grid contains the mid-Atlantic region, the entire northeastern United States east of
259 Indiana, parts of Canada, and a large area of the northern Atlantic Ocean. The 3-km grid contains the entire state of
260 Pennsylvania and most of the state of New York. Fifty vertical terrain-following model layers are used, with the centre point
261 of the lowest model layer located at ~10 m above ground level. The thickness of the layers stays nearly constant with height
262 within the lowest 1 kilometre, with 26 model layers below 850 hPa (~1550 m AGL). One-way nesting is used so that
263 information from the coarse domain translates to the fine domain but no information from the fine domain translates to the
264 coarse domain.

265 The WRF modelling system used for this study also has four-dimensional data assimilation (FDDA) capabilities to
266 allow meteorological observations to be assimilated into the model (Deng et al., 2009). With WRF FDDA, observations are
267 assimilated through the entire simulation to ensure the optimal model solutions that combine both observation and the
268 dynamic solution, a technique referred to as dynamic analysis. Data assimilation can be accomplished by nudging the model
269 solutions toward gridded analyses based on observations (analysis nudging), or directly toward the individual observations
270 (observation nudging), with a multiscale grid-nesting assimilation framework typically using a combination of these two
271 approaches (Deng et al., 2009; Rogers et al., 2013).

272 FDDA (Deng et al., 2009) was used in this research, with the same strategy as used in Rogers et al., (2013). Both
273 analysis nudging and observation nudging were applied on the 9-km grid, and only observation nudging was applied on the
274 3-km grid. In addition to assimilating observations and using the North America Regional Reanalysis model as initial
275 conditions, we reinitialize the WRF model every five days, allowing 12 hours of overlapping period in consideration of
276 model spin-up period to prevent model errors from growing over long periods. The observation data types assimilated
277 include standard WMO surface and upper-air observations distributed by the National Weather Service (NWS), available
278 hourly for surface and 12-hourly for upper air, and the Aircraft Communications Addressing and Reporting System

279 (ACARS) commercial aircraft observations, available anywhere in space and time with low-level observations near the
280 major airports.

281 The WRF model used in this study enables the chemical transport option within the model allowing for the
282 projection of CH₄ concentrations throughout the domain. Surface CH₄ emissions used as input for the model come from our
283 CH₄ emissions inventory and are all contained within the 3-km nested grid. Each source of CH₄ within our inventory is
284 defined with its own tracer (Table 1), allowing for the tracking of each individual source's contribution to the overall
285 projected CH₄ enhancement within the model. For this study, CH₄ is treated as an inert gas. The potential for interaction with
286 the hydroxyl radical (OH), the main sink of CH₄, is neglected. A calculation assuming an above-average OH mole fraction
287 over a rural region of 0.5 pptv (Stone et al., 2012) and a reaction rate of 6.5×10^{-15} (Overend et al., 1975) produces a CH₄ sink
288 of 0.5ppb per hour. The duration of a flight can be up to 3 hours, leading to a potential loss of 1.5ppb over the course of a
289 flight. This loss is small but not insignificant. CH₄ plumes associated with natural gas during each flight ranged between 15-
290 70 ppb, and a change of 1.5ppb could theoretically impact observations by as much as 10% of the plume signal. However,
291 this decrease in the CH₄ mole fraction would likely have equal impacts on both the background CH₄ values as well as the
292 enhancement. Because emission calculations are based on the relative difference between the CH₄ background mole fraction
293 and the enhancement downwind, it would take a gradient in the oxidation of OH to impact the results. Considering this
294 relatively low destruction rate, the expected homogeneity of the sink across the region, and the difficulties associated with
295 the simulation of chemical loss processes, we assumed that the CH₄ mass is conserved throughout the afternoon and
296 therefore we ignored the impact of oxidation by OH.

297

298 **2.4 Model Optimization Technique**

299 **2.4.1 Model Optimization Methodology**

300 The objective of the model optimization technique is to solve for an emission rate as a percent of natural gas production that
301 creates the best match between modelled CH₄ concentration maps, provided by the transport model, with actual CH₄ mole
302 fraction observations provided by the aircraft data. The optimization process in this study was originally designed to solve
303 for natural gas emission from unconventional wells and emissions from compressor facilities separately. Because the flow
304 rate of natural gas being processed was not available for each compressor station, emissions at each facility were originally
305 scaled based on the size of the station. However, when running the transport model using this emissions map, enhancements
306 from the compressor stations produced plume structures nearly identical in shape to enhancements from the unconventional
307 wells due to the similar spatial distributions of these two tracers. Without distinct differences between the enhancement
308 patterns from each tracer, it becomes impossible to distinguish which emissions source must be adjusted to obtain the closest
309 match to the observations. For this reason, emissions from compressor facilities are merged with unconventional well
310 emissions in the optimized emission rate. Though the emission rate solved for in this experiment only uses the locations and

311 production for the unconventional wells, this optimized rate represents emissions from both the wells and compressor
312 facilities and are referred to as the modelled upstream natural gas emission rate. Midstream and downstream natural gas
313 processes (such as processing, transmission and distribution of the gas) and emissions from conventional wells are not solved
314 for in this study due to their minimal contribution (less than 5%) to CH₄ emissions in the region encompassed by the aircraft
315 campaign.

316 Using the transport model WRF-Chem, CH₄ atmospheric enhancements were generated for each flight using
317 different tracers to track different components to the overall CH₄ enhancement (e.g. animal/animal waste, distribution sector,
318 industries). From these concentration fields, the upstream natural gas emission rate was solved for each flight using a three-
319 step model optimization technique. First, a background concentration was determined for each flight and subtracted from the
320 observations to create a set of “observed CH₄ enhancements,” using

$$321 \quad X_{EnhO} = X_{Obs} - X_{bg} \quad , \quad (1)$$

322 where X_{Obs} is the CH₄ mole fraction observation from the aircraft, X_{bg} is a chosen background value for the flight, and
323 X_{EnhO} is the calculated CH₄ enhancement at each observation. In this study, the background value is defined as the ambient
324 CH₄ mole fraction over the region not accounted for by any of the sources within the model, with each flight having a unique
325 background value. Box-pattern flights containing 2 loops around the basin may have a different background value assigned
326 for each loop. To determine the background mole fraction, we start with the value of the observed mole fraction in the lowest
327 2nd percentile of all observations within the boundary layer for a given flight or loop. This chosen background value
328 represents the CH₄ mole fraction across the flight path from sources that are outside of our model domain. Because the
329 background value is meant to represent the CH₄ mole fraction outside the model domain that is otherwise unaccounted for in
330 our model, using the observations with the lowest CH₄ mole fraction is not always a sufficient definition for the background.
331 On certain days, CH₄ enhancements from sources within the model domain can form plumes with wide spatial coverage that
332 cover all observations during a flight. For example, during a flight the lowest CH₄ observations from the aircraft may be
333 1850 ppb, but the model simulation during that period indicates that all observations within the flight are being impacted by
334 at minimum a 20 ppb enhancement. In this case, we would set our background value for the flight at 1830 ppb, and say that
335 our 1850 ppb observations from the flight are a combination of an 1830 ppb background in addition to a 20 ppb
336 enhancement from sources within the model. By subtracting off this background value from our observations, we create a set
337 of “observed CH₄ enhancements” which can be directly compared to the model projected enhancements

338 The next step is to remove enhancements from this set that are not associated with emissions from upstream natural
339 gas using

$$340 \quad X_{GasO} = X_{EnhO} - X_{OtherM} \quad , \quad (2)$$

341 where X_{OtherM} is the modelled CH₄ enhancement at each observation from sources unrelated to upstream natural gas
342 processes, and X_{GasO} is the observation-derived CH₄ enhancement associated with upstream natural gas emissions for each

343 observation. In this step, each observed CH₄ enhancement has subtracted from it the projected non-natural gas enhancement
344 from the model (i.e. nearest grid point in space) using the corresponding model output time closest to the observation within
345 a 20-minute time interval. This creates a set of observed CH₄ enhancements related only to emissions from upstream gas
346 processes, filtering out potential signals from other CH₄ emitters and providing a set of observed enhancements that can be
347 directly compared to the projected upstream natural gas enhancement within the model. By subtracting these other sources
348 from the observations, we make the assumption that our emissions inventory is accurate for non-natural gas sources and that
349 the transport of these emissions is perfect, both of which are actually uncertain. Because errors exist in both the emissions
350 and transport, it is possible to create a negative observation-derived upstream gas enhancement if model-projected
351 enhancements from other sources are larger than the observation-derived enhancement. From the 10 flights, 16% of the
352 observation-derived enhancements are negative, but only 3% are negative by more than 5 ppb. To avoid solving for
353 unrealistic negative values, these negative observation-based upstream gas enhancements are set to 0. Errors associated with
354 this issue and other uncertainties with our inventory are examined further in the uncertainly analysis section of this paper.

355 In the final step, the upstream natural gas emission rate within the model is adjusted to create the best match
356 between the modelled upstream gas enhancement and observation-derived upstream gas enhancement using

$$357 J = X_{GasO} - C * X_{GasM} \quad (3)$$

358 where X_{GasO} and X_{GasM} are the observed and modelled enhancement for each observation. In this equation, J is a cost
359 function we are trying to minimize by solving for a scalar multiplier C which, when applied to the modelled natural gas
360 enhancements, creates the smallest sum of the differences between the observation-derived upstream gas enhancement and
361 the modelled upstream enhancement. Because the emission rate within the model is linearly proportional to the model
362 enhancements, we can solve for the upstream natural gas emission rate that minimizes the cost function using

$$363 E = 0.13 C \quad (4)$$

364 where 0.13 was the first guess upstream emission rate (in percent of production) used in the model, and E is the optimized
365 emission rate for the flight as a percentage of the natural gas production at each well. This final value represents an overall
366 emission rate associated with both unconventional wells and compressor stations across the region.

367 The decision to use a scalar cost function rather than the sum of squares is to account for possible misalignment
368 between any observed CH₄ plume and modelled plumes. There are two potential ways in which misalignment may occur.
369 One possibility is that the modelled wind direction differs from the true wind direction, leading to a plume in the model that
370 is off-centre in relation to the observed plume. The other possibility relates to how the model treats emissions from natural
371 gas as a uniform percent of production. In reality the emissions are more random in nature, and thus the plume may not
372 always develop over the wells with the largest production values. If a cost function is used that minimizes the sum of the
373 squares, any misalignment between the modelled and observed plume will result in the peak of the modelled plume aligning
374 with the height of the tail of the observed plume (Figure 54). Unless the observed plume aligns perfectly with the modelled

375 plume, the optimized emission rate using a sum of squares approach will always bias low. By using a scalar cost function,
376 we solve for an optimized emission rate that results in a plume with the same area under the curve compared to the observed
377 plume (Figure 54). This methodology is not impacted by any misalignment between the modelled vs. observed plumes,
378 preventing the low biases associated with a sum of squares minimization.
379

380 2.4.2 Model Optimization Uncertainty Assessment

381 For each of the ten flights, an uncertainty assessment was performed to obtain a range of likely upstream emission rates for
382 any individual flight. Five different sources of error were considered in this assessment: model wind speed error, model
383 boundary layer height error, CH₄ background error, CH₄ emission inventory error, and model/observation mismatch error.
384 These five sources of error vary substantially from flight to flight depending on conditions, and each can have significant
385 impacts on the total uncertainty (Table 4, 5).

386 Errors in the modelled wind speed and boundary layer height have impacts on our emission estimates that linearly
387 impact the results. If we assume a constant wind speed, a constant boundary layer height, and no entrainment of air from the
388 top of the boundary layer, we can use the following equation to understand their impacts.

$$389 \Delta C = \bar{F}_0 \left(\frac{\Delta x}{U * D} \right) \quad (5)$$

390 where ΔC is the total CH₄ enhancement of the column of air contained within the boundary layer, \bar{F}_0 is the average emission
391 rate over the path the parcel travelled, Δx is the distance the column of air travelled, U is the wind speed and D is the
392 boundary layer height. Using this equation, we can see the linear relationship between the model wind speed, model
393 boundary layer height, and the calculated emission rate. As an example, if wind speeds in the model are biased low, natural
394 gas enhancements projected by the model would increase inversely. To compensate for this effect, the optimized emission
395 rate would decrease proportionally. A similar case can be made for bias in the boundary layer height. Both errors in the wind
396 speed and boundary layer height have known impacts on the optimized emission rate which can be corrected for, as long as
397 the errors of each are known.

398 To calculate the error in the model wind speed, we assume aircraft observations are truth and use

$$399 U_e = \frac{\bar{U}_m - \bar{U}_{obs}}{\bar{U}_{obs}} \quad (6)$$

400 where \bar{U}_{obs} is the mean observed wind speed by the aircraft across all points within the boundary layer, \bar{U}_m is the mean
401 modelled wind speed by the model across all points closest in time and space to each observation, and U_e is the wind speed
402 error percentage.

403 To compute the error in the modelled boundary layer height, the observed boundary layer height for each flight is
404 assumed to be the true boundary layer height and the boundary layer height percentage error, H_e , is estimated using:

405
$$H_e = \frac{H_m - \bar{H}_{obs}}{\bar{H}_{obs}} \quad (7)$$

406 where \bar{H}_{obs} is the average observed boundary layer height across each of the aircraft profiles for a given flight, \bar{H}_m is the
407 model boundary layer height closest in time and space to the location of the observed profiles averaged over all profiles. For
408 both the observation and the model, boundary layer heights were determined by locating height of the potential temperature
409 inversion associated with the top of the boundary layer. On the May 22 flight where a potential temperature inversion could
410 not easily be identified in the observations, changes in water vapour, CO₂ and CH₄ mixing ratios were used to identify the
411 boundary layer top.

412 Errors in the model wind speed and boundary layer height are calculated for each of the ten flights. From these
413 errors, a corrected optimized emission rate is calculated for each flight using Eq. (8):

414
$$E_{new} = \frac{E}{(1+U_e)(1+H_e)} \quad (8)$$

415 where E is the original emission rate and E_{new} is the corrected optimized upstream natural gas emission rate as a percent of
416 production.

417 In addition to errors related to wind speed and boundary layer height, we quantify three other sources of error in
418 each flight: errors in the selected CH₄ background value, errors in the CH₄ inventory, and errors associated with the overall
419 model performance (Table 5). Unlike the wind speed and boundary layer errors which have easily computable impacts on
420 the emission estimates, these other three sources of error and their impact on the optimized emission rate are more difficult
421 to quantify.

422 The background error relates to the value chosen for each flight which represents the ambient CH₄ concentration in
423 the boundary layer unrelated to emission sources within the model. In this study background values ranged from 1897-
424 1923ppb. Though background values should not have high variability during a 2-3 hour mid-afternoon flight, entrainment
425 from the boundary layer top can lead to the mixing in of tropospheric air that has different CH₄ mole fraction values from
426 those within the boundary layer, resulting in a change in the afternoon background value with time. Furthermore, for days on
427 which all aircraft observations (including those upwind of the unconventional wells) are impacted by various CH₄ plumes
428 predicted within the model, it is difficult to determine the background CH₄ concentration accurately. Additionally,
429 observations corresponding to locations with no modelled enhancement may in fact have been impacted by missing sources
430 in our inventory, highlighting the difficult nature of knowing with certainty where and what the background is for any given
431 flight. Understanding this uncertainty is crucial; any error in subtracting off the background value directly impacts each
432 observation's observed natural gas enhancement. For example, a background value of 1 ppb below the true background for a
433 given flight would add 1 ppb to each observed natural gas enhancement for all observations, creating a high bias with the
434 optimized upstream emission rate. To account for this error, each flight's optimization processes was rerun iterating the
435 background value by ± 5 ppb, and the ratio of the percent change in the emission rate compared to the original case was
436 defined as the resulting error in the emission rate due to background uncertainty. This ± 5 ppb background error range is an

437 estimate at the range of possible error in the background based on changes observed in the upwind measurements from each
438 of the flights and is meant to be a conservative estimate of the error. The impact this error can have in the emission rate
439 varies depending on the magnitude of the observed downwind enhancements during a flight. A plume containing a CH₄
440 enhancement of 50 ppb will have a smaller relative error from a 5 ppb change compared to one with an enhancement of only
441 10 ppb. Thus, days with high wind speeds and a high boundary layer height (and thus enhancements of a smaller magnitude)
442 tend to be affected the most by background errors.

443 Similar to background errors, errors from the CH₄ emissions inventory are difficult to quantify. In the model
444 optimization technique, we subtract out enhancements from sources unrelated to unconventional natural gas before solving
445 for the upstream gas emission rate. In doing so, we are making the assumption that our emissions inventory for sources
446 unrelated to upstream natural gas processes are accurate. In truth, each emission source in our inventory comes from a
447 different dataset and has its own unique error bounds, many of which are unknown. To simulate the potential errors
448 associated with unknowns in our inventory, we use a Monte Carlo approach and iterate the unconventional emissions
449 optimization approach for each flight 10,000 times, applying a random multiplier between 0-2 for each of the different
450 sources not associated with unconventional natural gas production. The resulting range of optimized natural gas emission
451 rates was fit to a Gaussian distribution and the 2σ emission range was calculated. Despite varying the emissions used in the
452 error analysis by 0 to 200% their original value, their impacts on the optimized natural gas emission rate are minimal on
453 most days due to the northeastern Marcellus region having very few emission sources not related to upstream natural gas
454 processes. Only for the flights on May 24th do we see errors from the inventory contribute significantly to the overall daily
455 error, when the coal plume in southwestern PA enters the centre of the study region and has a large role in the upstream
456 natural gas emission rate calculation for that day (Table 5).

457 The final source of error attempts to quantify the similarity of the pattern of modelled and observed natural gas
458 enhancements, referred to here as the model performance error. Figure 65 shows an example of two days, one of which the
459 model appears to recreate the observations, and the other of which the model poorly matches the shape of the observed
460 enhancements. Comparing these two simulations with no other information, we hypothesize that one should put more trust in
461 the upstream natural gas emission rate calculated for the flight whose modelled upstream enhancements match structurally
462 compared to the emission rate from the flight whose modelled enhancement bares little semblance to the observed
463 enhancement. The model performance error is designed to account for the trustworthiness of the optimized upstream
464 emission rate based on how well the model simulates a given day. The model performance error is calculated using a
465 modified normalized root mean squared error formula given in Eq. (9):

$$466 \quad e_{Perf} = \frac{\bar{\sigma}_{\Delta X}}{\Delta X_{gas}} \quad (9)$$

467 In this equation, $\bar{\sigma}_{\Delta X}$ is the standard deviation of the difference between the modelled and observation-derived upstream
468 natural gas CH₄ enhancement using the optimized emission rate, and ΔX_{gas} is the observed magnitude of enhancement from

469 the major natural gas plume observed in each flight. Here, ΔX_{gas} serves as a normalization factor to account for the varying
470 strength of the enhancement from flight to flight, and ensures that days with increased enhancements due to meteorological
471 conditions or true daily fluctuations in the upstream natural gas emissions do not proportionally impact the performance
472 error percentage. For example, a day with high winds and a deep boundary layer would produce smaller enhancements,
473 leading to a small $\bar{\sigma}_{\Delta X}$ regardless of model performance unless normalized by ΔX_{gas} .
474

475 2.5 Aircraft Mass Balance Method and Uncertainty Assessment

476 An aircraft mass balance calculation was performed for four applicable flights from the aircraft campaign as an alternative
477 method to calculate upstream natural gas emission rates independent of the transport model. The aircraft mass balance
478 approach uses the CH₄ enhancement between a downwind and upwind transect to calculate the total CH₄ flux of the area
479 contained between the two transects. We use the mass balance equation from Karion et al., (2013):

$$480 \quad E = \bar{U} \cos(\bar{\theta}) \int_{-b}^b \Delta X \int_{z=0}^{z_{top}} n_{air} dz dx \quad (10)$$

481 where E is the total flux (in mol s⁻¹) coming from the enclosed flight track, \bar{U} is the mean wind speed (in m s⁻¹), $\bar{\theta}$ is the mean
482 angle of the wind perpendicular to the flight track, ΔX is the CH₄ enhancement measured along the downwind flight track
483 from $-b$ to b (expressed as a mole fraction), n_{air} is the molar density of air within the boundary layer (in mol m⁻³), and each
484 of the integrals represents the summing over all air being measured within our transect in both the horizontal (x) and the
485 vertical (z). By simplifying further and using the mean enhancement along each downwind transect as the enhancement and
486 choosing z_{top} to be the top of the boundary layer, we can transform the previous equation into the following:

$$487 \quad E = 37.3 L D U \bar{\Delta X} \cos(\bar{\theta}) \quad (11)$$

488 where L is the length of the transect (in meters), D is the depth of the boundary layer (in meters) found using observations
489 from vertical ascents during each flight, $\bar{\Delta X}$ is the mean enhancement across the transect (expressed as a mole fraction), \bar{U}
490 and $\bar{\theta}$ are the mean wind speed (in m s⁻¹) and wind direction relative to the angle of the transect, and 37.3 is the average
491 molar density of dry air within the boundary layer (in mol m⁻³) assuming an average temperature and pressure of 290K and
492 900hPa.

493 Of the 6 days from the aircraft campaign with a clearly defined upwind and downwind transect, one day (May 14th)
494 contained a surface high-pressure centre in the middle of the flight resulting in erratic wind patterns, and another day (May
495 25th) had CH₄ plumes from southwestern PA affecting portions the flight observations. These days were not used for a mass
496 balance, and calculations were performed for the remaining four box-pattern flights (May 22nd, May 23rd, May 28th, May
497 29th). From this list of remaining flights, three of them contained two loops around a portion of the Marcellus basin. A mass
498 balance was performed on each loop, resulting in a total of 7 mass balance calculations for the region across 4 days. Table 6
499 summarizes the results from the mass balance flights.

500 For each flight, a total flux within the box encompassed was calculated using Eq. (11). Using this flux, a natural gas
501 emission rate based on production from within the box was calculated using Eq. (12)

$$502 \quad E_{\%} = \frac{E - E_{other}}{P} \quad (12)$$

503 where E is the total flux from Eq. (11) (in kg hr^{-1}), E_{other} are the emissions enclosed in the box from sources not
504 related to upstream natural gas processes (in kg hr^{-1}), P is the total CH_4 from natural gas being produced within the box (in
505 kg hr^{-1}), and $E_{\%}$ is the resulting natural gas emission rate as a percent of total production within the box.

506 As an error analysis for the mass balance flight, we look at four potential sources of error (Table 7). One source of
507 uncertainty comes from the observed wind speed used in Eq. (11). For our experiment, we take the mean observed wind
508 speed from the aircraft and assume this value represents the mean wind speed within the entire box during the 2-4 hour
509 period it would take for air to travel from the upwind transect to the downwind transect. To understand the uncertainty and
510 biases associated with this assumption, we recreate wind observations along the flight path using values from WRF-Chem,
511 and compare the mean wind speed from the simulated observations to the mean model winds contained within the box
512 integrated throughout the boundary layer during the 3 hour period closest to the flight time. By making this comparison, we
513 are able to understand the representation error associated with treating the wind speed observations from the aircraft as the
514 wind speed within the entire box during the period it would take for air to cross from the upwind transect to the downwind
515 transect. On average, modelled wind speeds following the flight were 7% faster than integrated wind speeds within the box,
516 due to the inability for aircraft observations to account for slower wind speeds closer to the surface. This bias was removed
517 from each day's calculated wind speed. After accounting for the wind speed bias, the average error of the modelled wind
518 speed following the flight path compared to the modelled winds within the box was 3%. This 3% uncertainty was applied to
519 each flight and used as the potential uncertainty in the mean wind speed. Errors in the wind direction were neglected, as each
520 flight used in the mass balance completely surrounded the basin using downwind transects at multiple angles, and thus small
521 errors in the wind angle would result in a negligible net change on the total flux calculated.

522 Another source of uncertainty is error in the boundary layer height. For each flight, between 2-3 vertical profiles
523 were performed, and the mean height was used in Eq. (11). The standard deviation of different heights from each transect
524 was used as the uncertainty. On May 22nd, a boundary layer height could be interpreted from only one vertical transect. For
525 this day, we assume an uncertainty of ± 200 m ($\pm 9\%$).

526 Uncertainty in the CH_4 background mole fraction was estimated similar to the boundary layer height. On three of
527 the four flights, two upwind transects were performed. The mean observed CH_4 mole fraction between the two transects was
528 used as the background value for the entire flight, and the standard deviation between the loops was used as the uncertainty.
529 On both the May 23rd and May 28th flights, background differences between the two transects were less than the instrument
530 error of 1 ppb. On these days, we use the instrument error as the background error. On May 22nd, only one upwind transect
531 was usable for the calculation. For this day, we assume a conservative estimate in the uncertainty of the background of ± 5
532 ppb.

533 Finally, we assess uncertainty in the emissions inventory. After a CH₄ flux is calculated for each loop, emissions
534 from sources contained within the box that are not associated with upstream natural gas processes must be subtracted out to
535 solve for the upstream natural gas emission rate. Any errors associated with our inventory will result in a CH₄ source
536 attribution error. To account for the potentially large uncertainty with the emission sources in our inventory, we vary these
537 non-natural gas emissions by a factor of 2 to test the impact on the solved upstream natural gas emission rate. Because
538 northeastern Pennsylvania contains few sources of CH₄ emissions outside of natural gas production, the impact of this
539 uncertainty is typically less than 20% of the total emissions calculated within the box.

540 **3 Results**

541 **3.1 Methane Inventory**

542 From the first-guess CH₄ inventory created in this study, a total anthropogenic CH₄ emission rate of 2.76 Tg CH₄ year⁻¹ is
543 projected within our inner model domain (Figure 76) with values for individual source contributions shown in Table 2. This
544 total emissions estimate assumes a leak rate of 0.13% of gas production for unconventional wells, and does not account for
545 emissions from natural gas transmission and storage facilities outside of PA due to a lack of information available from other
546 states. Within the model domain, the area encompassing southwestern PA and northeastern WV stands out as the largest
547 contributor to CH₄ emissions, with emissions from conventional gas, unconventional gas, and coal mines all having
548 significant contributions to the total. In particular, the large emissions from coal make this region unique in comparison to
549 other shales. The EPA's Greenhouse Gas Reporting Program dataset for the year 2014 lists individual coal mines in the
550 southwestern portion of our domain as 8 of the top 10 CH₄ emitting facilities across the entire United States. This large area
551 source of CH₄ can have an impact on CH₄ concentrations hundreds of kilometres downwind and must be taken into account
552 when winds are from the southwest (Figure 87). Examples of this plume and its impacts on the aircraft campaign are
553 discussed in Section 3.2.1.

554

555 **3.2 Model Optimization Results**

556 **3.2.1 Case Studies**

557 From the aircraft campaign, a total of 10 flights across 9 days were used in the model optimization technique. For each one
558 of these flights, CH₄ concentration fields were produced using WRF-Chem, and the emission rate from upstream gas
559 processes was adjusted as outlined in the methods section to find the rate that best matches the total observed CH₄
560 enhancement. For box flights with two loops completed around the basin, emission rates were calculated for each loop
561 independent from one another and then averaged for the flight. Table 3 provides the general meteorology for the 10 flights.

562 During each of the observational periods, we use the transport model to project the mole fraction enhancement
563 across the region for each of the different CH₄ tracers (Figure 98). From these projections, we see three common sources of
564 CH₄ which can significantly influence the observed mole fractions in our study region of northeastern PA. The first is
565 emissions from unconventional gas in northeastern PA. Although the first-guess total emissions from upstream production in
566 the Marcellus are small compared to the overall contributions from other sources within the domain, their proximity to the
567 aircraft track results in unconventional gas having the largest contribution to observed enhancements throughout the domain
568 covered by most of the flights, often producing signals downwind of about 20-80 ppb above background levels. The second
569 most influential source of enhancements in our study region comes from various sources of CH₄ emissions located in
570 southwestern PA. Despite being more than 400 km away from our study region, large plumes from coal and other sources in
571 the southwestern corner of the state can contribute enhancements as high as 50 ppb across portions of the flight when winds
572 are from the southwest, affecting background measurements and masking signals from the unconventional gas. One final,
573 but less influential source of CH₄ enhancement is animal agriculture in southeastern PA. Lancaster County is home to
574 roughly 20% of all cattle in the state, with more than 200,000 cattle and calves as of 2012. A southerly wind can result in a
575 5-15 ppb enhancement across the flight path due to enteric fermentation and manure management from these cattle. Because
576 of coal, conventional gas, and cattle sources located south of the basin, signals from flights with a southerly component to
577 the wind can be difficult to interpret without modelling the projected plumes associated with these sources. Observations on
578 these days contrast to days with a northerly wind component, where a lack of CH₄ sources north of the study region results in
579 observations with a more clearly defined background and unconventional natural gas enhancement.

580 For each of the ten flights, variability in the model-observation offset was observed. The first loop of the May 29th
581 flight is the best example of a case where comparisons between the modelled and observed enhancements match closely after
582 optimization. For this flight, a box pattern was flown encompassing a majority of the unconventional wells in northeastern
583 PA, and enhancements were observed along the western and northern transects of the flight. Modelled enhancements from
584 sources unrelated to upstream gas emissions showed a broad CH₄ plume associated mostly with animal agriculture along the
585 western edge of the flight, and a smaller enhancement on the eastern edge associated with two landfills in the
586 Scranton/Wilkes-Barre urban corridor (Figure 109). Both of these enhancements are subtracted off from the observations to
587 produce a set of observation-derived enhancements due to upstream natural gas production and gathering facilities. Any
588 enhancements in this new observational dataset are located almost entirely along the northern transect of the flight, directly
589 downwind of the natural gas activity in the region. The observation-derived upstream gas enhancement is then directly
590 compared to the modelled upstream enhancement using its first guess emission rate, and an optimized upstream emission
591 rate of 0.26% of production (i.e. a doubling of the first guess) is calculated by minimizing the difference between the two
592 datasets (Figure 110).

593 The match between observed and modelled CH₄ enhancements on the first loop of the May 29th flight is closer than
594 any other flight in the campaign. The success of the model on this day is likely due to a number of ideal conditions. In
595 general, inconsistencies between the modelled and observed mean wind speeds and boundary layer heights can have a linear

596 bias on the projected enhancements, but for this flight differences between the observed and modelled wind speed and
597 boundary layer height were near 0 for both loops (Figure 11, 12, 13). Observed wind directions throughout the course of the
598 flight had little directional spread and the averaged observed wind direction was only 9° different compared to modelled
599 values, resulting in a transport of the CH₄ plumes that the model was able to match well. Furthermore, the observed mean
600 wind speed was 4.6 m s⁻¹, a moderate wind which allows for a steady transport of any enhancements towards the downwind
601 transect, but not strong enough to dilute their magnitude, resulting in an easily observable enhancement downwind of the
602 basin. Finally, intrusions from sources unrelated to upstream gas were small on this day due to favourable wind conditions,
603 reducing the probability of incorrectly attributing the observed enhancements to the wrong source. Enhancements from
604 upstream natural gas processes were between 15-40 ppb along our downwind transect. By comparison, enhancements from
605 other sources were lower than 15 ppb along a majority of the flight, and most of these enhancements were located west of
606 the downwind transect, making them easier to identify and remove without unintentionally impacting enhancements from the
607 natural gas plume. All of these different factors likely contributed to producing a situation where the model was successfully
608 able to match CH₄ observations during the May 29th flight.

609 Flights that occurred on days with a southwest wind had a tendency to produce CH₄ observations that were
610 intuitively difficult to interpret due to convolved CH₄ sources in southwestern Pennsylvania. One of these complex
611 observation sets occurred during the late afternoon flight on May 24th, 2015 (Figure 14, 13). Observations on this day show a
612 CH₄ enhancement that decreased with latitude, with higher CH₄ mole fractions observed farther south. Given the location of
613 the wells in the middle of the flight path and the WSW wind pattern in the region, this north/south CH₄ gradient is
614 unexpected and counterintuitive compared to where one would expect the enhancements to be based solely on the presence
615 of the gas industry in northeastern PA. However, through modelling each of the many contributors of CH₄ within our
616 inventory, we are able to recreate this latitudinal CH₄ gradient and better understand the observed patterns (Figure 14, 13).
617 Throughout an 18-hour period leading up to the May 24th flight, winds from the SSW transport emissions from coal in
618 southwestern PA northeastward until they reach the centre of the state, where a westerly wind then shifts the plume across
619 the study region such that it only intersects the southern half of the flight path. Because of both the magnitude of the coal
620 emissions and an accumulation that occurred in the southwestern portion of the state during the previous night, the modelled
621 enhancement from the coal plume is substantial (>20 ppb) as it crosses over the flight path and covers up much of the signal
622 from upstream gas emissions. Nonetheless, the transport model is able to account for these far-reaching sources and attempt
623 to separate out their contribution to the observed enhancements. We are able to recreate the May 24th flight observations
624 more accurately than most other flights, with a correlation coefficient of 0.71 between the observations and model CH₄
625 values. Although the model successfully recreates the overall observed CH₄ pattern on this flight, attempting to match model
626 vs. observation-derived enhancements specifically from upstream natural gas contributions is much more difficult.
627 Contributions from non-natural natural gas sources are large such that they overwhelm much of the signal from local natural
628 gas sources. After subtracting out non-natural gas sources from the observations, the correlation specifically between
629 modelled and observation-derived upstream natural gas enhancements is only 0.11.

630 Despite the model's success at recreating observations from the May 24th late-afternoon flight, there is reason to be
631 careful when interpreting results on day with observations influenced by distant sources. In particular, some transport error is
632 unavoidable in atmospheric reanalyses, and the longer the time and distance a plume takes to reach the observations, the
633 more its position and magnitude will be susceptible to these errors. During the early May 24th flight, a small 50 km shift in
634 the location of the coal plume across the study region would change projected enhancements at some observations by as
635 much as 20 ppb. Furthermore, errors in the transport speed could create scenarios where the coal plume either arrives in the
636 study region too early or exits too late, creating a projected enhancement pattern that does not agree with the observations
637 (Figure ~~+514~~). Additionally, inaccuracies with the emission estimates of non-unconventional gas sources in the inventory
638 will impact the magnitude of their CH₄ enhancements, creating additional errors in the optimization process when
639 subtracting out these enhancements from the observations. The early-afternoon May 24th flight and May 25th flight are both
640 examples where influences from CH₄ sources in southwest PA create complex structures in the enhancements, which the
641 model is not able to match as well as the late-afternoon flight on May 24th (Figure ~~+615~~). And although observations and
642 modelled enhancements closely match throughout portions of these two flights, a slight shift in the modelled wind direction
643 can lead to vastly differing results due to the large offset small changes in the wind field can have on an emission source
644 hundreds of kilometres away. Thus, results from the flights on May 24th and May 25th should be taken with caution. A deeper
645 analysis of these errors can be found in Section 3.2.2.

646 3.2.2 Emission Rates and Uncertainty Assessment

647 Table 4 shows the wind speed and boundary layer height errors for each flight as well as the optimized and
648 corrected natural gas emission rates. On days where model performance was poor in regards to the wind speed and boundary
649 layer height, we can see changes in the corrected emission rate. For most days, this change is less than 20% different than the
650 original optimized emission rate. However, both May 14th and May 25th have corrected emission rates which are around a
651 factor of 2 different from their original value. Whether these corrected emission rates are more accurate than the original
652 optimized rates is debatable. To calculate these alternative emission rates, we must assume that the wind speeds and
653 boundary layer heights from our limited number of observations are the true values in the atmosphere, which may not be the
654 case. Regardless of which rate is more accurate for each flight, the overall 16% high bias in the model wind speed and the
655 -12% low bias in the model boundary layer result in compensating errors that cancel out, and the mean emission rates across
656 all flights end up similar. Thus, any errors associated with these two meteorological variables has a trivial impact on the
657 overall calculated emission rate for the region and the uncorrected emission rates are used for the final mean and uncertainty
658 calculations.

659 Table 5 summarizes the background error, inventory error, and model performance error, and assumes
660 independence between the three error sources to calculate the total uncertainty for each flight. The largest uncertainty exists
661 for the May 22nd flight, where an unexplained enhancement along the northern transect led to a poor match between the
662 modelled enhancements and the observed enhancements. This may explain the anomalously high optimized emission rate for

663 that day. Other flights with large uncertainty are those that occurred on May 24th, where enhancements from southwestern
664 PA are believed to be influencing large portions of the observations.

665 Based on the conservative methodology used to calculate these uncertainties, we assume the total uncertainty for
666 each flight represents a 2σ range of possible emission rates and calculate a weighted mean and a 2σ confidence interval for
667 the overall upstream emission rate across the ten flights. From this approach, we find a mean upstream emission rate of
668 0.36% of production and a 2σ confidence interval from 0.27-0.45% of production.

669 3.3 Aircraft Mass Balance Results

670 Calculated emission rates varied extensively between flights used for the mass balance analysis, ranging from 0.11% to
671 1.04% of natural gas production (Table 6). Comparing emission rates between loops on the same day, we see more
672 consistency in the values. This result is not surprising, as on each of the days with multiple loops, upwind and downwind
673 CH₄ concentrations patterns tended to be similar between loops. Thus, differences in the total emission rate are likely due to
674 either errors specific to each day (such as background variability, errors in meteorology) or real daily variability in the
675 upstream natural gas emission rate.

676 From Table 7, we can see the largest error with regards to the absolute uncertainty in the emission rate occurs on the
677 May 22nd flight. It is on this day where we have the largest uncertainty in the background value, with observations towards
678 the end of the flight becoming unusable due to a rapid and unexplained decrease in the CH₄ mole fraction of 8 ppb over a 30
679 minute period (Figure 4716). This day also features the highest boundary layer height and fastest winds of all flights done in
680 this study, reducing the magnitude of the enhancement associated with the natural gas plume and thus amplifying the effects
681 an uncertain background has on the overall uncertainty of the calculated CH₄ flux. Uncertainty across the other three flights
682 is smaller, and results between individual loops on the May 23rd and May 28th flight provide more confidence in the
683 calculated flux for those days.

684 Using the mean estimated CH₄ emissions and uncertainty for each loop, we calculate a daily mean emission rate and
685 uncertainty for each of the four days. We then solve for an unweighted mean across the four flights to derive our overall
686 emissions estimate from the aircraft mass balance approach, and use the standard error of the flights to estimate the
687 uncertainty. In doing so, we derive a natural gas emission rate from upstream processes of 0.40% of production, with a 2σ
688 confidence interval from 0.08-0.72% of production. Here, we use the arithmetic mean rather than a weighted mean due to the
689 linear relationship between the size of the emission rate and the size of the errors. Because errors associated with ABL height
690 and wind speed have a proportional impact on the calculated emissions within the box, days with a high emissions estimate
691 produce large uncertainties relative to days with a small emission rate. Using a weighted mean approach assigns more weight
692 to the days with low estimated emissions, and produces an overall emission estimate too low and certain to have confidence
693 in (0.12±0.02 percent of gas production).

694

695 **4 Discussion**

696 **4.1 Upstream Emission Rate**

697 From this study, we estimate with a 2σ confidence interval an emission rate between 0.27-0.45% of gas production using the
698 model optimization method and ~~0.0608-0.6272~~ 0.4817% of gas production using the aircraft mass balance. Figure 4817 provides the
699 emission range estimates from upstream natural gas processes using both the model optimization technique and mass balance
700 technique when applicable. Top-down studies of other basins in the U.S. have all found emission rates greater than 1% of
701 production, and thus the rates calculated for the northeastern Marcellus basin are the lowest observed yet, raising questions
702 as to why the values in this region appear to be low. One possibility may be related to the well efficiency of the northeastern
703 Marcellus region compared to other major shale plays (Table 8). In terms of gas production per unconventional well, the
704 Marcellus is the highest of all major basins in the U.S. Furthermore, the gas production per well increases by nearly a factor
705 of two when focusing specifically on Susquehanna and Bradford Counties in northeastern Pennsylvania where the majority
706 of the wells from this study are located (Figure 1). The large difference in production per well between the northeastern
707 Marcellus and other shales may partly explain the low emission rates as a percentage of production. Throughout this study,
708 we normalize natural gas emissions as a percentage of total production under the assumption that higher throughput of
709 natural gas in a system should lead to higher emissions in the system. However, if leaks are more influenced by the number
710 of components in operation rather than the throughput passing through the wells, a high production-per-well system such as
711 the unconventional wells in the northeastern Marcellus could end up having a very low emission rate as a percentage of
712 production, but a similar emission rate compared to other basins based on the number of wells, compressors, etc. A thorough
713 bottom-up study of the Marcellus region measuring emissions on a device level could provide an answer to this hypothesis.

714 Although we calculate a low emission rate for this region, rates calculated for May 22 and May 25 stand out as
715 outliers where emissions fall well-above our uncertainty bounds. It is possible that emissions from natural gas sources were
716 higher on these days compared to others. Releases of natural gas into the atmosphere from short timeframe events such as
717 liquids unloading and venting can add a temporal component to the emission rate. Such events occurring at an increased
718 frequency during the May 22 and May 25 flights could be responsible for the higher emission rates. However, these two days
719 both have issues that could have affected the optimized emission rate. On May 22, we observe a sudden drop in the observed
720 CH₄ values that is nearly as large as the main plume on that day, creating concerns about background concentrations. On
721 May 25, a southwesterly wind was present, and while the model showed the coal plume to be west of the flight path, a small
722 shift in the model wind direction would shift the coal plume over the region. For these reasons we are sceptical but not
723 dismissive of the high emission rates found during these two flights.

724

725

726 4.2 Advantages of Combining Observations with Model Output

727 One of the major advantages of using a chemical transport model to solve for natural gas emission rates compared to a
728 standard mass-balance approach is that the transport model is able to account for the complex and oftentimes non-uniform
729 plume structures originating from sources outside the flight path that can affect observations. When performing a mass
730 balance over a basin, it is assumed that the upwind transect is representative of the air exiting the downwind transect after
731 subtracting out all sources within the box. However, this assumption is only true if winds contained within the flight path are
732 in perfect steady state during the time it take for air to move from the upwind transect to the downwind transect, and that
733 measurements from the downwind transect occurred at a much later time so that the air being measured is the same air
734 measured from the upwind transect. These conditions are not easily achieved for regional scale mass balances due to the long
735 times needed for the air from the upwind transect to reach the downwind transect. As an example, from the four mass
736 balance flights performed for this study the average time for air to move from the upwind transect to the downwind transect
737 was 4 hours whereas the average time between the aircraft's upwind and downwind measurements was ~40 minutes. The
738 aircraft observations can be thought of as a snapshot in time, which can be problematic if large scale plumes from outside the
739 domain are moving through the region and impacting only certain portions of the observations during the flight's short
740 timeframe. By using a transport model for a domain much larger than that of the flight paths, we are able to track these far-
741 reaching plumes and identify situations where the background CH₄ concentrations may be spatially heterogeneous.

742 The potential usefulness of using a transport model alongside a mass balance calculation can best be demonstrated
743 from observations taken over the Marcellus during a 2013 aircraft campaign (Peischl et. al 2015). During this flight the
744 prevailing winds were from the WSW, and the largest CH₄ enhancements were observed along the western edge of the flight
745 path, upwind of the unconventional wells. Using our transport model, we are able to recreate the day of flight and attempt to
746 use our inventory and explain this feature (Figure 4918). Comparisons between modelled output and observations show a 60
747 ppb CH₄ enhancement from coal and conventional wells in southwest PA stretching close to the western edge of the aircraft
748 observations, a plume structure similar to the one observed during the May 24th flight from our own study. Though this
749 plume does not initially align with the observed transect with the largest enhancements, we recognize that the coal and gas
750 plume travels for more than 20 hours (a distance of 400 km) from its source before reaching the flight path. If we allow for a
751 10% error in the transport speed and therefore advance the transport model by an additional two hours past the time in which
752 the aircraft observed these high values, we are able to line up the centre of the plume with the largest observed CH₄ mole
753 fractions along the western edge of the flight. In addition to the 60 ppb enhancement along the centre of the plume, the
754 model projects 20 ppb enhancements along the edges and in front of the plume centre. These smaller enhancements have an
755 influence along different portions of the flight which varies in magnitude, making it difficult to assess a proper background
756 CH₄ value upwind of the wells and potentially masking natural gas enhancements downwind of them. But by using a
757 transport model, we are able to see the potential impact of these far-reaching sources which would otherwise not be

758 considered in a regional mass balance and better understand the complex CH₄ plume structures which can occur in a given
759 region under specific wind conditions.

760 **5 Conclusion**

761 Using the model optimization technique presented in this study, we find a weighted mean natural gas emission rate from
762 unconventional production and gathering facilities of 0.36% of production with a 2 σ confidence interval from 0.27-0.45% of
763 production. This emission rate is supported by four mass balance calculations, which produce a mean of 0.40% and a 2 σ
764 confidence interval from of 0.08-0.72% of production. Applied to all the wells in our study region, this mean rate results in a
765 leakage rate of 20 Mg CH₄ hr⁻¹ for the year 2015. The emission rate found in this top-down study quantified as a percent of
766 production is significantly lower than rates found using top-down methodology at any other basin, and indicates the presence
767 of some fundamental difference in the northeastern Marcellus gas industry that is resulting in more efficient extraction and
768 processing of the natural gas.

769 The ten flights that took place in this study reveal large regional variations in the CH₄ enhancement patterns
770 depending on the prevailing wind direction. On days with a northwest wind, observed enhancements come primarily from
771 natural gas sources, and a small plume associated with it can be seen on the downwind leg of each flight with few
772 enhancements upwind of the wells. Flights that took place with winds conditions predominantly from the southwest were
773 more difficult to interpret. Plumes associated with coal and other potential sources of CH₄ in the southwestern Pennsylvania
774 create complex enhancement patterns affecting both the upwind and downwind portions of the flight, making both the
775 background CH₄ mole fraction and enhancements from the gas industry difficult to interpret. The stark difference between
776 observations that occurred with a northwest wind compared to a southwest wind illustrates the importance of having multiple
777 flights across days with various wind conditions to better understand the major influences on CH₄ concentrations throughout
778 a region. The regional influences in Pennsylvania also demonstrate the utility of deriving an emissions inventory that
779 provides input data to drive a transport model, allowing one to forecast CH₄ mole fractions on difficult days and better
780 understand the daily uncertainties associated with heterogeneous background conditions.

781 Though this study presented observations from ten flights over a three-week period, it is not able to account for the
782 potential of long term temporal variability in the emission rates. In May 2015 when the flights took place, the entire
783 Marcellus basin was nearing peak production and active drilling and hydraulic fracturing was still ongoing in the region. By
784 mid-2016, the rate of drilling of new wells in the northeast Marcellus had decreased and natural gas production had begun to
785 decline in the area. A snapshot of the emission rate during one month of a basin in its peak production is insufficient to
786 characterize emissions from an area that is likely to be producing and transporting gas at various intensities for decades. We
787 need to quantify the long-term climatological impacts of gas production. Future work examining the temporal variability of
788 CH₄ emissions within natural gas basins would complement short-term, high-intensity studies such as this one, and aid with
789 understanding how well the calculated emission rates represent the gas basin over the course of time.

790 **Acknowledgements**

791 This work has been funded by the U.S. Department of Energy National Energy Technology Laboratory (project DE-
792 FE0013590). We thank in-kind contributions from the Global Monitoring Division of the National Oceanic and Atmospheric
793 Administration, and from the Earth and Environmental Systems Institute, the Department of Meteorology and Atmospheric
794 Science, and the College of Earth and Mineral Science of The Pennsylvania State University. We also want to thank the
795 Pennsylvania College of Technology in Williamsport, PA for access to their Technology Aviation Center facilities during
796 the aircraft campaign. We also want to thank Lillie Langlois from the Department of Ecosystem Science and
797 Management for sharing pipeline information, Anthony J. Marchese and Dan Zimmerle (Colorado State University) for
798 information on compressor stations, Jeff Peischl for sharing data from his 2013 flight campaign, and Bernd Haupt (Penn
799 State University) for data processing and management during the project. We thank the two anonymous reviewers who
800 volunteered their time to improve the contents of this paper. Finally, we would like to thank Dennis and Joan Thomson for
801 their creation and continued support of the Thomson Distinguished Graduate Fellowship.

802 **References**

- 803 Alvarez, R. A., Pacala, S. W., Winebrake, J. J., Chameides, W. L., and Hamburg, S. P.: Greater focus needed on methane
804 leakage from natural gas infrastructure, *Proceedings of the National Academy of Sciences*, 109, 6435-6440,
805 10.1073/pnas.1202407109, 2012.
- 806
- 807 Bloom, A. A., Bowman, K., Lee, M., Turner, A. J., Schroeder, R., Worden, J. R., Weidner, R., McDonald, K. C., and Jacob,
808 D. J.: A global wetland methane emissions and uncertainty dataset for atmospheric chemical transport models,
809 *Geosci. Model Dev.*, 10.5194/gmd-10-2141-2017, 2017.
- 810
- 811 Bradford County: Maps of Natural Gas Development in Bradford County, available at:
812 <http://www.bradfordcountypa.org/index.php/natural-gas-information>.
- 813
- 814 Bousquet, P., Ciais, P., Miller, J. B., Dlugokencky, E. J., Hauglustaine, D. A., Prigent, C., Van der Werf, G. R., Peylin, P.,
815 Brunke, E. G., Carouge, C., Langenfelds, R. L., Lathiere, J., Papa, F., Ramonet, M., Schmidt, M., Steele, L. P.,
816 Tyler, S. C., and White, J.: Contribution of anthropogenic and natural sources to atmospheric methane variability,
817 *Nature*, 443, 439-443, http://www.nature.com/nature/journal/v443/n7110/supinfo/nature05132_S1.html, 2006.
- 818
- 819 Brandt, A. R., Heath, G. A., Kort, E. A., O'Sullivan, F., Pétron, G., Jordaan, S. M., Tans, P., Wilcox, J., Gopstein, A. M.,
820 Arent, D., Wofsy, S., Brown, N. J., Bradley, R., Stucky, G. D., Eardley, D., and Harriss, R.: Methane Leaks from
821 North American Natural Gas Systems, *Science*, 343, 733-735, 10.1126/science.1247045, 2014.
- 822
- 823 Cambaliza, M. O. L., Shepson, P. B., Caulton, D. R., Stirm, B., Samarov, D., Gurney, K. R., Turnbull, J., Davis, K. J.,
824 Possolo, A., Karion, A., Sweeney, C., Moser, B., Hendricks, A., Lauvaux, T., Mays, K., Whetstone, J., Huang, J.,
825 Razlivanov, I., Miles, N. L., and Richardson, S. J.: Assessment of uncertainties of an aircraft-based mass balance
826 approach for quantifying urban greenhouse gas emissions, *Atmos. Chem. Phys.*, 14, 9029-9050, 10.5194/acp-14-
827 9029-2014, 2014.
- 828
- 829 Chen, F., and Dudhia, J.: Coupling an Advanced Land Surface-Hydrology Model with the Penn State-NCAR MM5
830 Modeling System. Part I: Model Implementation and Sensitivity, *Monthly Weather Review*, 129, 569-585,
831 10.1175/1520-0493(2001)129<0569:caalsh>2.0.co;2, 2001.
- 832
- 833 Conley, S., Franco, G., Faloona, I., Blake, D. R., Peischl, J., and Ryerson, T. B.: Methane emissions from the 2015 Aliso
834 Canyon blowout in Los Angeles, CA, *Science*, 10.1126/science.aaf2348, 2016.
- 835
- 836 Deng, A., Stauffer, D., Gaudet, B., Dudhia, J., Hacker, J., Bruyere, C., Wu, W., Vandenbergh, F., Liu, Y., and Bourgeois,
837 A.: Update on WRF-ARW end-to-end multi-scale FDDA system, 10th Annual WRF Users' Workshop, Boulder,
838 CO, June 23, 2009.
- 839
- 840 Deng, A., Gaudet, B., Dudhia, J., and Alapaty, K.: Implementation and Evaluation of a New Shallow Convection Scheme in
841 WRF, 94th American Meteorological Society Annual Meeting, Atlanta, GA, February 2-6, 2014.
- 842
- 843 EIA: Annual Energy Outlook 2012 with Projections to 2035, available at:
844 [http://www.eia.gov/forecasts/aeo/pdf/0383\(2012\).pdf](http://www.eia.gov/forecasts/aeo/pdf/0383(2012).pdf), 2012.
- 845
- 846 EIA: Layer Information for Interactive State Maps, available at: https://www.eia.gov/maps/layer_info-m.cfm, 2015
- 847
- 848 EIA: Shale in the United States, available at: https://www.eia.gov/energyexplained/index.cfm?page=natural_gas_where,
849 2016a
- 850

851 EIA: Monthly Energy Review: June 2016. [Available online at
852 <http://www.eia.gov/totalenergy/data/monthly/archive/00351607.pdf>, 2016b.
853

854 EPA: Abandoned Coal Mine Methane Opportunities Database, available at: [https://www.epa.gov/cmop/abandoned-](https://www.epa.gov/cmop/abandoned-underground-mines)
855 [underground-mines](https://www.epa.gov/cmop/abandoned-underground-mines), 2008.
856

857 EPA: Greenhouse Gas Reporting Program 2014, available at: [https://www.epa.gov/ghgreporting/ghg-reporting-program-](https://www.epa.gov/ghgreporting/ghg-reporting-program-data-sets)
858 [data-sets](https://www.epa.gov/ghgreporting/ghg-reporting-program-data-sets), 2015a.
859

860 EPA: Inventory of US Greenhouse Gas Emissions and Sinks: 1990-2013 Annex 3.6, available at:
861 <https://www.epa.gov/ghgemissions/inventory-us-greenhouse-gas-emissions-and-sinks-1990-2013>, 2015b.
862

863 EPA: Inventory of US Greenhouse Gas Emissions and Sinks: 1990-2014 Annex 2.2, available at:
864 <https://www.epa.gov/ghgemissions/inventory-us-greenhouse-gas-emissions-and-sinks-1990-2014>, 2016.
865

866 Frankenberg C., Thorpe, A. K., Thompson, D. R., Hulley, G., Kort, E. A., Vance, N., Borchardt, J., Krings, T., Gerilowski,
867 K., Sweeney, C., Conley, S., Bue, B. D., Aubrey, A. D., Hook, S., and Green, R. O.: Airborne methane remote
868 measurements reveal heavy-tail flux distribution in Four Corners region, *Proceedings of the National Academy of*
869 *Sciences*, 113, 9734-9739, 2016.
870

871 Hughes, J. D.: *Drilling Deeper: A Reality Check on US Government Forecasts for a Lasting Tight Oil & Shale Gas Boom*,
872 Post Carbon Institute, Santa Rosa, California, 2014.
873

874 Iacono, M. J., Delamere, J. S., Mlawer, E. J., Shephard, M. W., Clough, S. A., and Collins, W. D.: Radiative forcing by long-
875 lived greenhouse gases: Calculations with the AER radiative transfer models, *Journal of Geophysical Research:*
876 *Atmospheres*, 113, 10.1029/2008jd009944, 2008.
877

878 Jimenez, P. A., Hacker, J. P., Dudhia, J., Haupt, S. E., Ruiz-Arias, J. A., Gueymard, C. A., Thompson, G., Eidhammer, T.,
879 and Deng, A.: WRF-Solar: Description and Clear-Sky Assessment of an Augmented NWP Model for Solar Power
880 Prediction, *Bulletin of the American Meteorological Society*, 97, 1249-1264, 10.1175/bams-d-14-00279.1, 2016.
881

882 Jiménez, P. A., Alessandrini, S., Haupt, S. E., Deng, A., Kosovic, B., Lee, J. A., and Monache, L. D.: The Role of
883 Unresolved Clouds on Short-Range Global Horizontal Irradiance Predictability, *Monthly Weather Review*, 144,
884 3099-3107, 10.1175/mwr-d-16-0104.1, 2016.
885

886 Kain, J. S., and Fritsch, J. M.: A One-Dimensional Entraining/Detraining Plume Model and Its Application in Convective
887 Parameterization, *Journal of the Atmospheric Sciences*, 47, 2784-2802, 10.1175/1520-
888 0469(1990)047<2784:aodepm>2.0.co;2, 1990.
889

890 Kain, J. S.: The Kain-Fritsch Convective Parameterization: An Update, *Journal of Applied Meteorology*, 43, 170-181,
891 10.1175/1520-0450(2004)043<0170:tkcpau>2.0.co;2, 2004.
892

893 Karion, A., Sweeney, C., Pétron, G., Frost, G., Michael Hardesty, R., Kofler, J., Miller, B. R., Newberger, T., Wolter, S.,
894 Banta, R., Brewer, A., Dlugokencky, E., Lang, P., Montzka, S. A., Schnell, R., Tans, P., Trainer, M., Zamora, R.,
895 and Conley, S.: Methane emissions estimate from airborne measurements over a western United States natural gas
896 field, *Geophysical Research Letters*, 40, 4393-4397, 10.1002/grl.50811, 2013.
897

898 Karion, A., Sweeney, C., Kort, E. A., Shepson, P. B., Brewer, A., Cambaliza, M., Conley, S. A., Davis, K., Deng, A.,
899 Hardesty, M., Herndon, S. C., Lauvaux, T., Lavoie, T., Lyon, D., Newberger, T., Pétron, G., Rella, C., Smith, M.,

900 Wolter, S., Yacovitch, T. I., and Tans, P.: Aircraft-Based Estimate of Total Methane Emissions from the Barnett
901 Shale Region, *Environmental Science & Technology*, 49, 8124-8131, 10.1021/acs.est.5b00217, 2015.
902

903 Lamb, B. K., Cambaliza, M. O. L., Davis, K. J., Edburg, S. L., Ferrara, T. W., Floerchinger, C., Heimbürger, A. M. F.,
904 Herndon, S., Lauvaux, T., Lavoie, T., Lyon, D. R., Miles, N., Prasad, K. R., Richardson, S., Roscioli, J. R., Salmon,
905 O. E., Shepson, P. B., Stirm, B. H., and Whetstone, J.: Direct and Indirect Measurements and Modeling of Methane
906 Emissions in Indianapolis, Indiana, *Environmental Science & Technology*, 50, 8910-8917,
907 10.1021/acs.est.6b01198, 2016.
908

909 Langlois, L. A., Drohan, P. J., and Brittingham, M. C.: Linear infrastructure drives habitat conversion and forest
910 fragmentation associated with Marcellus shale gas development in a forested landscape. *Journal of Environmental*
911 *Management*. 197, 167-176, 10.1016/j.jenvman.2017.03.045. 2017.
912

913 Lauvaux, T., Uliasz, M., Sarrat, C., Chevallier, F., Bousquet, P., Lac, C., Davis, K. J., Ciais, P., Denning, A. S., and Rayner,
914 P. J.: Mesoscale inversion: first results from the CERES campaign with synthetic data, *Atmos. Chem. Phys.*, 8,
915 3459-3471, 10.5194/acp-8-3459-2008, 2008.
916

917 Maasakkers, J. D., Jacob, D. J., Sulprizio, M. P., Turner, A. J., Weitz, M., Wirth, T., Hight, C., DeFigueiredo, M., Desai, M.,
918 Schmeltz, R., Hockstad, L., Bloom, A. A., Bowman, K. W., Jeong, S., and Fischer, M. L.: Gridded National
919 Inventory of U.S. Methane Emissions, *Environmental Science & Technology*, 50, 13123-13133,
920 10.1021/acs.est.6b02878, 2016.
921

922 Marchese, A. J., Vaughn, T. L., Zimmerle, D. J., Martinez, D. M., Williams, L. L., Robinson, A. L., Mitchell, A. L.,
923 Subramanian, R., Tkacik, D. S., Roscioli, J. R., and Herndon, S. C.: Methane Emissions from United States Natural
924 Gas Gathering and Processing, *Environmental Science & Technology*, 49, 10718-10727, 10.1021/acs.est.5b02275,
925 2015.
926

927 Mays, K. L., Shepson, P. B., Stirm, B. H., Karion, A., Sweeney, C., and Gurney, K. R.: Aircraft-Based Measurements of the
928 Carbon Footprint of Indianapolis, *Environmental Science & Technology*, 43, 7816-7823, 10.1021/es901326b, 2009.
929

930 Mlawer, E. J., Taubman, S. J., Brown, P. D., Iacono, M. J., and Clough, S. A.: Radiative transfer for inhomogeneous
931 atmospheres: RRTM, a validated correlated-k model for the longwave, *Journal of Geophysical Research:*
932 *Atmospheres*, 102, 16663-16682, 10.1029/97jd00237, 1997.
933

934 Myhre, G., Shindell, D., Bréon, F.-M., Collins, W., Fuglestedt, J., Huang, J., Koch, D., Lamarque, J.-F., Lee, D., and
935 Mendoza, B.: Anthropogenic and natural radiative forcing, *Climate change*, 423, 2013.
936

937 Nakanishi, M., and Niino, H.: An improved Mellor–Yamada level-3 model: Its numerical stability and application to a
938 regional prediction of advection fog, *Boundary-Layer Meteorology*, 119, 397-407, 2006.
939

940 NYDEC: NY 2014 Oil & Gas Production Data: available at: <http://www.dec.ny.gov/energy/36159.html>, 2016.
941

942 Omara, M., Sullivan, M. R., Li, X., Subramanian, R., Robinson, A. L., and Presto, A. A.: Methane Emissions from
943 Conventional and Unconventional Natural Gas Production Sites in the Marcellus Shale Basin, *Environmental*
944 *Science & Technology*, 50, 2099-2107, 10.1021/acs.est.5b05503, 2016.
945

946 Overend, R. P., Paraskevopoulos, G., and Cvetanović, R. J.: Rates of OH Radical Reactions. I. Reactions with H₂, CH₄,
947 C₂H₆, and C₃H₈ at 295 K, *Canadian Journal of Chemistry*, 53, 3374-3382, 10.1139/v75-482, 1975.
948

949 PADEP: PA Oil and Gas Well Historical Production Report, available at:
950 http://www.depreportingservices.state.pa.us/ReportServer/Pages/ReportViewer.aspx?%2fOil_Gas%2fOil_Gas_Wel
951 [l_Historical_Production_Report](http://www.depreportingservices.state.pa.us/ReportServer/Pages/ReportViewer.aspx?%2fOil_Gas%2fOil_Gas_Wel), 2016.
952

953 Peischl, J., Ryerson, T. B., Aikin, K. C., de Gouw, J. A., Gilman, J. B., Holloway, J. S., Lerner, B. M., Nadkarni, R.,
954 Neuman, J. A., Nowak, J. B., Trainer, M., Warneke, C., and Parrish, D. D.: Quantifying atmospheric methane
955 emissions from the Haynesville, Fayetteville, and northeastern Marcellus shale gas production regions, *Journal of*
956 *Geophysical Research: Atmospheres*, 120, 2119-2139, 10.1002/2014jd022697, 2015.
957

958 Pétron, G., Frost, G., Miller, B. R., Hirsch, A. I., Montzka, S. A., Karion, A., Trainer, M., Sweeney, C., Andrews, A. E.,
959 Miller, L., Kofler, J., Bar-Ilan, A., Dlugokencky, E. J., Patrick, L., Moore, C. T., Ryerson, T. B., Siso, C.,
960 Kolodzey, W., Lang, P. M., Conway, T., Novelli, P., Masarie, K., Hall, B., Guenther, D., Kitzis, D., Miller, J.,
961 Welsh, D., Wolfe, D., Neff, W., and Tans, P.: Hydrocarbon emissions characterization in the Colorado Front Range:
962 A pilot study, *Journal of Geophysical Research: Atmospheres*, 117, 10.1029/2011jd016360, 2012.
963

964 Platts: Maps and Geospatial Data: available at: <http://www.platts.com/maps-geospatial>, 2016.
965

966 Rogers, R., Deng, A., Stauffer, D., Jia, Y., Soong, S., Tanrikulu, S., Beaver, S., and Tran, C.: Fine particulate matter
967 modeling in Central California. Part I: Application of the Weather Research and Forecasting model, 91th Annual
968 Meeting, 2011.
969

970 Ryerson, T. B., Trainer, M., Holloway, J. S., Parrish, D. D., Huey, L. G., Sueper, D. T., Frost, G. J., Donnelly, S. G.,
971 Schaufli, S., Atlas, E. L., Kuster, W. C., Goldan, P. D., Hübler, G., Meagher, J. F., and Fehsenfeld, F. C.:
972 Observations of Ozone Formation in Power Plant Plumes and Implications for Ozone Control Strategies, *Science*,
973 292, 719-723, 10.1126/science.1058113, 2001.
974

975 Schwietzke, S., Griffin, W. M., Matthews, H. S., and Bruhwiler, L. M. P.: Natural Gas Fugitive Emissions Rates Constrained
976 by Global Atmospheric Methane and Ethane, *Environmental Science & Technology*, 48, 7714-7722,
977 10.1021/es501204c, 2014.
978

979 Smith, M. L., Kort, E. A., Karion, A., Sweeney, C., Herndon, S. C., and Yacovitch, T. I.: Airborne Ethane Observations in
980 the Barnett Shale: Quantification of Ethane Flux and Attribution of Methane Emissions, *Environmental Science &*
981 *Technology*, 49, 8158-8166, 10.1021/acs.est.5b00219, 2015.
982

983 Skamarock, W. C., Klemp, J. B., Dudhia, J., Gill, D. O., Barker, D. M., Wang, W., and Powers, J. G.: A description of the
984 advanced research WRF version 2, DTIC Document, 2005.
985

986 Stone, D., Whalley, L. K., and Heard, D. E.: Tropospheric OH and HO₂ radicals: field measurements and model
987 comparisons, *Chemical Society Reviews*, 41, 6348-6404, 10.1039/c2cs35140d, 2012.
988

989 Sweeney, C., Karion, A., Kort, E. A., Smith, M. L., Newberger T., Schwietzke, S., Wolter, S., and Lauvaux, T.: Aircraft
990 Campaign Data over the Northeastern Marcellus Shale, May-June 2015, Version: 2017-03-29, Path:
991 <https://doi.org/10.15138/G35K54>, 2015
992

993 Tewari, M., Chen, F., Wang, W., Dudhia, J., LeMone, M., Mitchell, K., Ek, M., Gayno, G., Wegiel, J., and Cuenca, R.:
994 Implementation and verification of the unified NOAA land surface model in the WRF model, 20th conference on
995 weather analysis and forecasting/16th conference on numerical weather prediction, 2004.
996

997 Thompson, G., Field, P. R., Rasmussen, R. M., and Hall, W. D.: Explicit Forecasts of Winter Precipitation Using an
998 Improved Bulk Microphysics Scheme. Part II: Implementation of a New Snow Parameterization, Monthly Weather
999 Review, 136, 5095-5115, 10.1175/2008mwr2387.1, 2008.
1000
1001 USDA: Census Ag Atlas Maps, available at:
1002 https://www.agcensus.usda.gov/Publications/2012/Online_Resources/Ag_Atlas_Maps/Livestock_and_Animals/,
1003 2012.
1004
1005 White, W. H., Anderson, J. A., Blumenthal, D. L., and Wilson, W. E., Formation and transport of secondary air-pollutants:
1006 Ozone and aerosols in St. Louis urban plume: Science 194, 187-189, 10.1126/science.959846, 1976.
1007
1008 WVDEP: WV Oil and Gas Database and Map Information, available at: [http://www.dep.wv.gov/oil-and-](http://www.dep.wv.gov/oil-and-gas/databaseinfo/Pages/default.aspx)
1009 [gas/databaseinfo/Pages/default.aspx](http://www.dep.wv.gov/oil-and-gas/databaseinfo/Pages/default.aspx), 2016.
1010
1011 Zavala-Araiza, D., Lyon, D., Alvarez, R. A., Palacios, V., Harriss, R., Lan, X., Talbot, R., and Hamburg, S. P.: Toward a
1012 Functional Definition of Methane Super-Emitters: Application to Natural Gas Production Sites, Environmental
1013 Science & Technology, 49, 8167-8174, 10.1021/acs.est.5b00133, 2015
1014
1015 Zavala-Araiza, D., Alvarez, R. A., Lyon, D. R., Allen, D. T., Marchese, A. J., Zimmerle, D. J., and Hamburg, S. P.: Super-
1016 emitters in natural gas infrastructure are caused by abnormal process conditions, Nature Communications, 8, 14012,
1017 10.1038/ncomms14012, 2017.
1018
1019 Zimmerle, D. J., Williams, L. L., Vaughn, T. L., Quinn, C., Subramanian, R., Duggan, G. P., Willson, B., Opsomer, J. D.,
1020 Marchese, A. J., Martinez, D. M., and Robinson, A. L.: Methane Emissions from the Natural Gas Transmission and
1021 Storage System in the United States, Environmental Science & Technology, 49, 9374-9383,
1022 10.1021/acs.est.5b01669, 2015.

Table 1: List of tracers used in the transport model.

Tracer #	Name	Description of source
1	Unconventional Wells	Emissions from unconventional wells.
2	Storage Facilities	Emissions from compressors associated with natural gas storage.
3	Pipelines	Emissions from gathering and transmission pipelines
4	Distribution	Emissions from the distribution sector of the natural gas industry.
5	Conventional Wells	Emissions from conventional wells.
6	Landfills/Other	Emissions from landfills and uncharacterized industrial sources.
7	Coal	Emissions from active and abandoned coal mining.
8	Animals/Waste	Emissions from enteric fermentation and manure management
9	Production Compressors (HP)	Emissions from compressor stations characterized as “production”. Emissions scaled linearly with wattage.
10	Gathering Compressors (HP)	Emissions from compressor stations characterized as “gathering”. Emissions scaled linearly with wattage.
11	Other Compressors (HP)	Emissions from all other compressor stations. Emissions scaled linearly with wattage.
12	Production Compressors (C)	Emissions from compressor stations characterized as “production”. Emissions constant among compressors.
13	Gathering Compressors (C)	Emissions from compressor stations characterized as “gathering”. Emissions constant among compressors.
14	Other Compressors (C)	Emissions from all other compressor stations. Emissions constant among compressors.

Table 2: Annual emission rate totals from anthropogenic sources within the innermost model domain based on values from the inventory within this study

Source	Total Emission Rate (Gg CH ₄ year ⁻¹)
Unconventional Wells	125
Conventional Wells	607
Gathering Compressor Facilities	118
Storage Facilities	69
Gathering/Transmission Pipelines	8
Natural Gas Distribution	213
Underground, Surface, and Abandoned Coal Mines	831
Enteric Fermentation/Manure Management	371
Landfills	420
Total	2762

Table 3: Meteorological statistics from the May 2015 flight campaign.

Day	Flight Pattern	# of Loops	# of Vertical Profiles	ABL Depth (m)	Mean Observed Wind Speed (m/s)	Mean Observed Wind Direction	Model Background Value (ppm)
May 14	Box	1	2	1300	2.9	30°	1.908
May 21	Raster	N/A	2	1300	3.9	231°	1.905
May 22	Box	2	2	2300	10.1	300°	1.910
May 23	Box	2	2	1400	4.4	276°	1.906
May 24 ¹	Other	N/A	2	1500	4.4	270°	1.923
May 24 ²	Raster	N/A	2	2050	4.8	272°	1.907
May 25	Box	1	2	1800	9.0	217°	1.920
May 28	Box	2	3	1400	7.1	322°	1.897
May 29	Box	2	2	1000	4.6	195°	1.899
June 3	Raster	N/A	1	1250	2.7	149°	1.898

Table 4: Optimized natural gas emission rates for each flight as well as corrected emission rates adjusting for errors in the model wind speed and boundary layer height. For wind speed and boundary layer height error, a negative value represents a model value less than the observations.

Day	Optimized NG Emission Rate (% of production)	Wind Speed Error (6)	Boundary Layer Height Error (7)	Corrected NG Emission Rate (% of production)
May 14	0.37	-31%	-33%	0.80
May 21	0.53	3%	39%	0.37
May 22	1.15	37%	-18%	1.02
May 23	0.45	34%	-9%	0.37
May 24	0.68	48%	-21%	0.58
May 24	0.36	48%	-21%	0.30
May 25	0.99	3%	-43%	1.69
May 28	0.33	-4%	-8%	0.37
May 29	0.35	4%	1%	0.33
June 3	0.26	19%	-8%	0.24
Average	0.55	16%	-12%	0.61

Table 5: Emission rates and potential errors associated with the model optimization technique. r-values represent the correlation between the model and observation-derived upstream natural gas enhancements.

Day	Optimized Upstream Emission Rate (% of production)	r-value Model vs Obs NG Sources	Background Error	Non-Upstream Gas Inventory Error	Model Performance Error	Total Error	2 σ Confidence Interval (% of Production)
May 14	0.37	0.20	$\pm 24\%$	$\pm 19\%$	$\pm 17\%$	$\pm 35\%$	± 0.13
May 21	0.53	0.31	$\pm 24\%$	$\pm 13\%$	$\pm 30\%$	$\pm 41\%$	± 0.22
May 22	1.15	0.47	$\pm 38\%$	$\pm 5\%$	$\pm 37\%$	$\pm 53\%$	± 0.61
May 23	0.45	0.10	$\pm 39\%$	$\pm 13\%$	$\pm 42\%$	$\pm 59\%$	± 0.26
May 24 ¹	0.68	0.31	$\pm 24\%$	$\pm 81\%$	$\pm 17\%$	$\pm 86\%$	± 0.58
May 24 ²	0.36	0.11	$\pm 51\%$	$\pm 150\%$	$\pm 31\%$	$\pm 161\%$	± 0.57
May 25	0.99	0.43	$\pm 29\%$	$\pm 15\%$	$\pm 30\%$	$\pm 44\%$	± 0.44
May 28	0.33	0.33	$\pm 76\%$	$\pm 12\%$	$\pm 20\%$	$\pm 79\%$	± 0.26
May 29	0.35	0.58	$\pm 24\%$	$\pm 11\%$	$\pm 19\%$	$\pm 33\%$	± 0.12
June 3	0.26	0.37	$\pm 31\%$	$\pm 12\%$	$\pm 24\%$	$\pm 41\%$	± 0.11

Table 6: Emission rates from mass balance calculations on applicable days, with emission ranges associated with a ± 5 ppb error in the background value.

Flight	CH ₄ Production within box (Gg hr ⁻¹)	Mass Balance CH ₄ Flux (kg hr ⁻¹)	Non-Upstream CH ₄ Emissions (kg hr ⁻¹)	Calculated Upstream Emission Rate (% of production)	2 σ Confidence Interval (% of Production)
May 22 ₁	4.96	53800	2250	1.04	± 1.09
May 22 ₂	4.96	27400	2250	0.51	± 1.08
May 23 ₁	4.05	5600	934	0.11	± 0.07
May 23 ₂	4.05	5500	934	0.11	± 0.07
May 28 ₁	3.73	7100	706	0.17	± 0.11
May 28 ₂	3.73	6000	843	0.14	± 0.10
May 29 ₁	4.63	27900	1622	0.57	± 0.30

Table 7: Relative error associated with the different sources of uncertainty in the aircraft mass balance.

Flight	Wind Speed Error	Background Error	ABL Error	Inventory Error	Total Error (1σ)	Upstream Emission Rate (% of Production) w/ 2σ Confidence Interval
May 22 ₁	±3%	±56%	±9%	±5%	±57%	1.04 ±1.09
May 22 ₂	±3%	±121%	±9%	±8%	±121%	0.51 ±1.08
May 23 ₁	±3%	±24%	±7%	±20%	±32%	0.11 ±0.07
May 23 ₂	±3%	±26%	±7%	±21%	±34%	0.11 ±0.07
May 28 ₁	±3%	±31%	±7%	±11%	±34%	0.17 ±0.11
May 28 ₂	±3%	±33%	±7%	±16%	±38%	0.14 ±0.10
May 29 ₁	±3%	±28%	±20%	±8%	±36%	0.57 ±0.30

Table 8: Production statistics from mid-2014 for various shales across the United States (Hughes 2014).

	Barnett	Fayetteville	Haynesville	Marcellus	Bradford/ Susquehanna County, PA
# of Producing Wells	16100	4500	3100	7000	1558
Total Production (Bcf day ⁻¹)	5.0	2.8	4.5	12	5.01
Production per well (MMcf day ⁻¹)	0.31	0.56	1.25	1.71	3.22

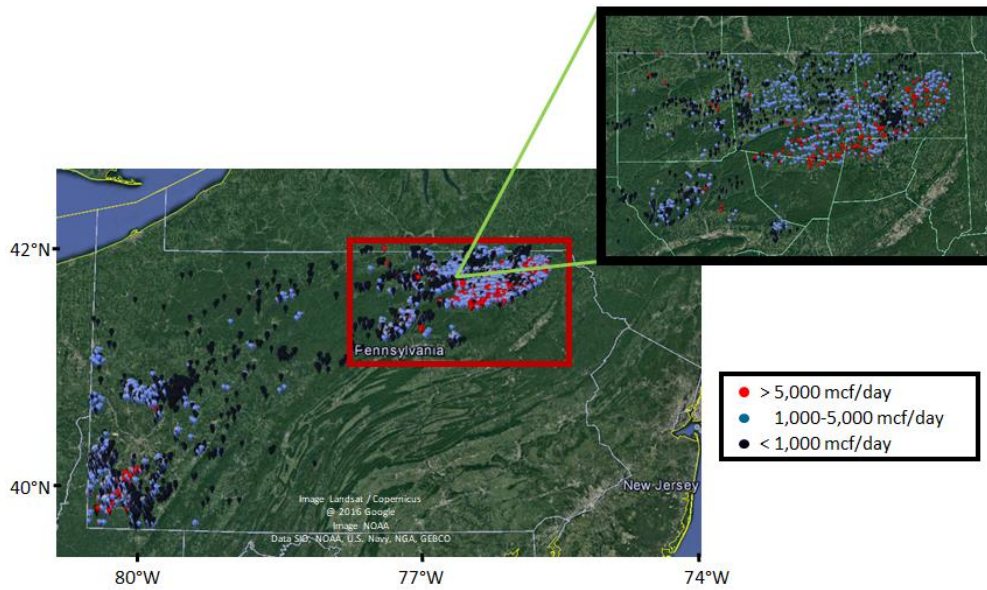


Figure 1: A map of the unconventional wells in Pennsylvania dotted in purple. Production values of wells for May 2015 are indicated by the marker colour. Red rectangle and zoom-in show the region of focus for this study, 41.1-42.2°N 75.2-77.6°W.

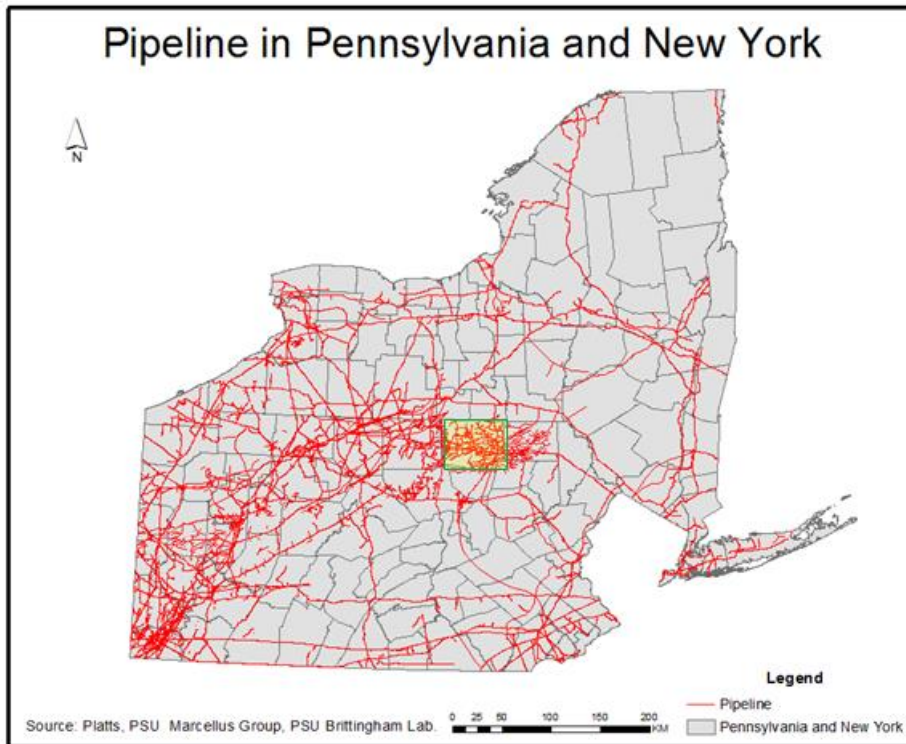


Figure 2: A map of transmission and gathering pipelines for the state of PA and NY. Transmission pipelines are provided by Platts Natural Gas Pipelines product. Gathering pipelines associated with unconventional wells in PA are extrapolated using information on existing gathering pipelines provided by Bradford County, PA (highlighted in yellow).

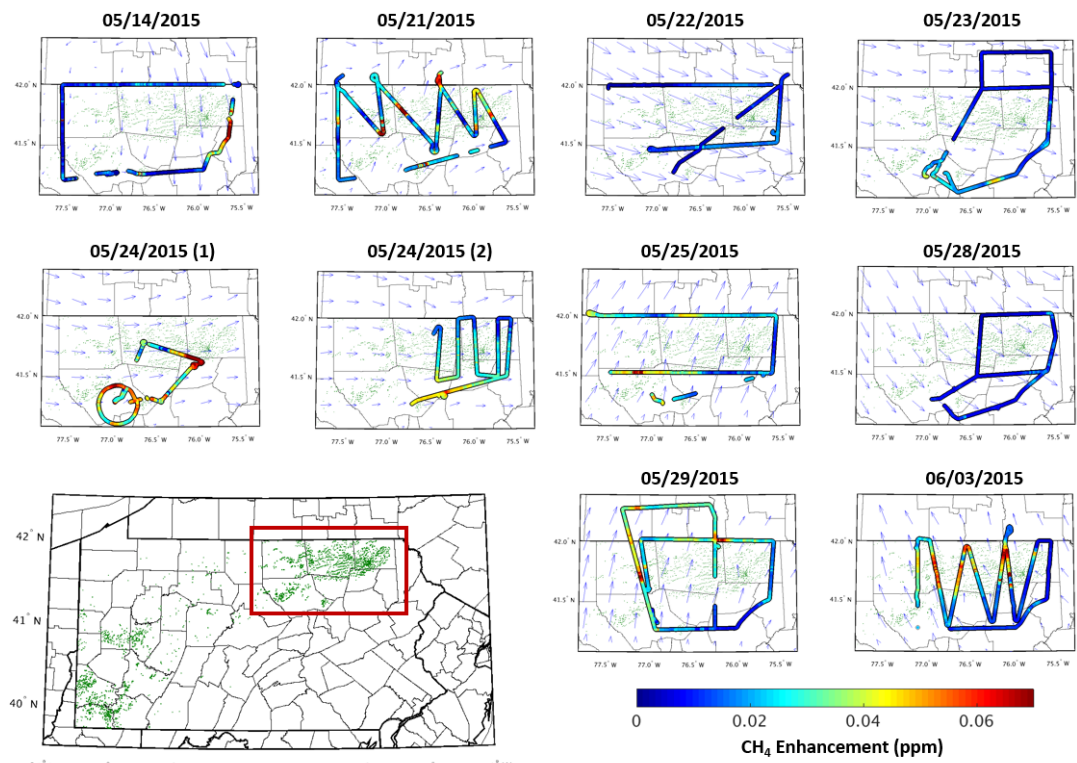


Figure 3: Observed CH₄ enhancements within the boundary layer from each of the 10 afternoon flights used in this study, with green dots showing the location of unconventional wells in PA and blue arrows showing the modelled wind direction during the time of the flight. CH₄ enhancements are calculated by taking the observed CH₄ mole fraction values and subtracting off the flight's background CH₄ value shown in Table 3.

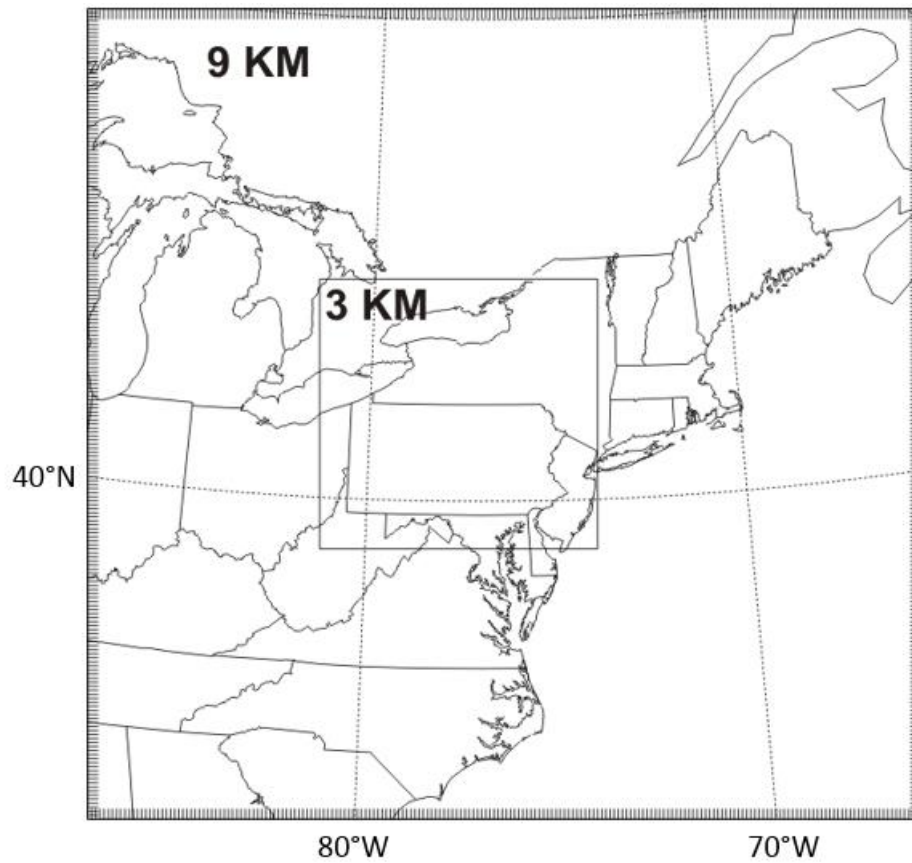


Figure 4: Model domain and resolutions used within the transport model. All emissions used for this study are contained within the 3-km resolution domain.

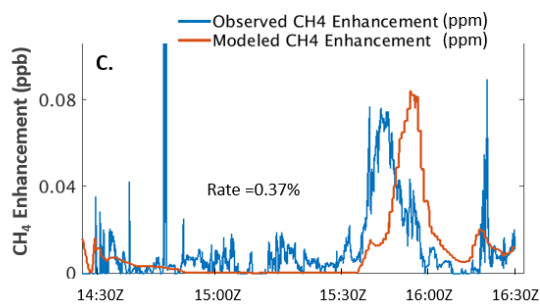
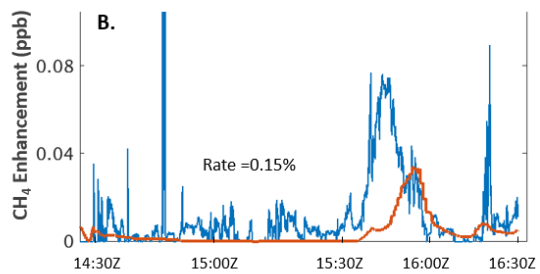
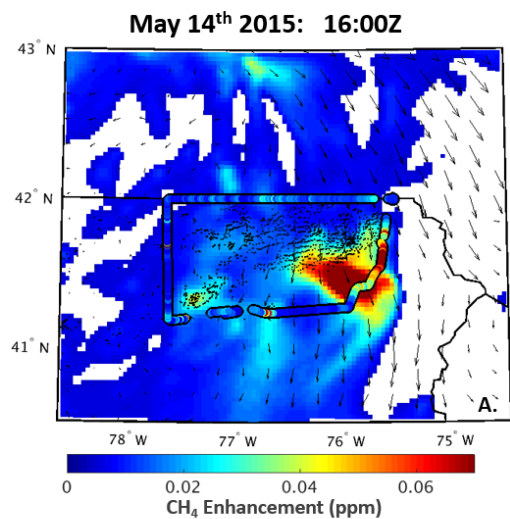


Figure 5: (a.)

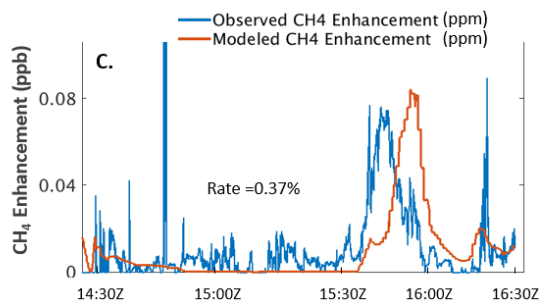
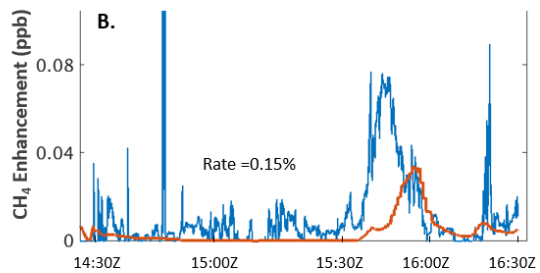
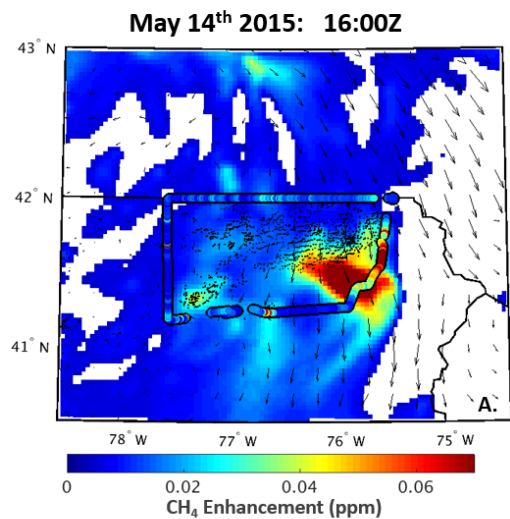


Figure 4: (a.) Observed vs model projected CH₄ enhancements during the May 14th, 2015 at 16Z. (b.) Comparison of observed natural gas enhancement to modelled natural gas enhancement along flight path, with upstream emission rate optimized by minimizing the absolute error between the datasets. (c.) Same as previous, but optimized by minimizing the sum of the error between the datasets.

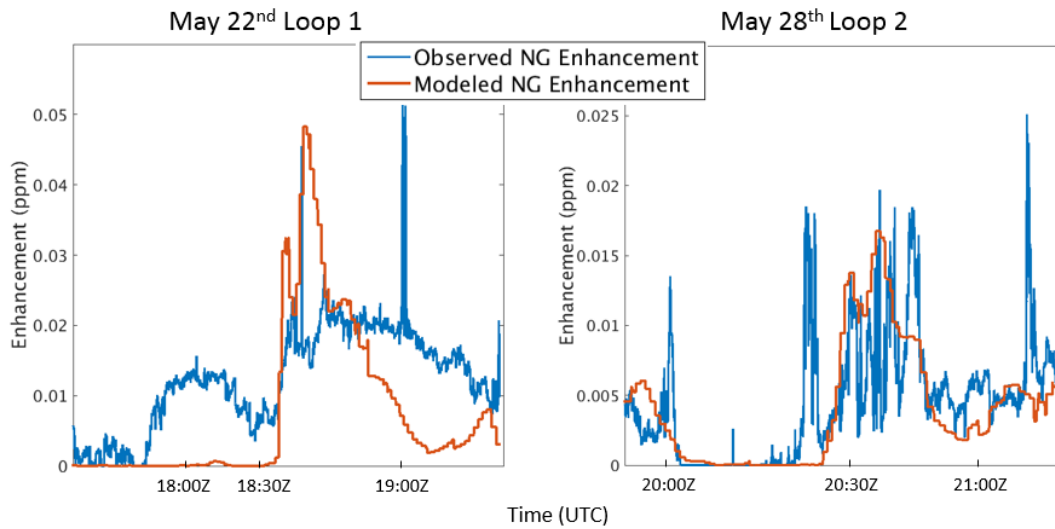


Figure 65: Comparison of observed natural gas enhancement to modelled natural gas enhancement for segments along the (left) May 22nd flight and (right) May 28th flight. A distinct lack of representativeness of the observations in the modelled enhancement can be seen in the May 22nd flight compared to the May 28th flight.

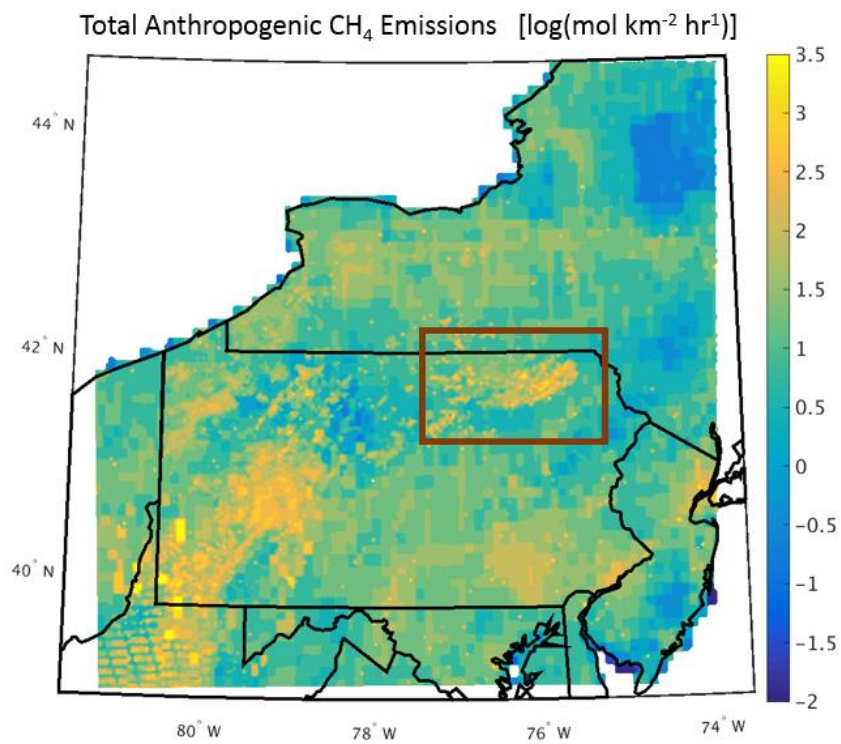


Figure 76: A log scale contour of the anthropogenic CH₄ emissions inventory from this study used within the transport model. The red rectangle surrounds the study region where the aircraft campaign took place.

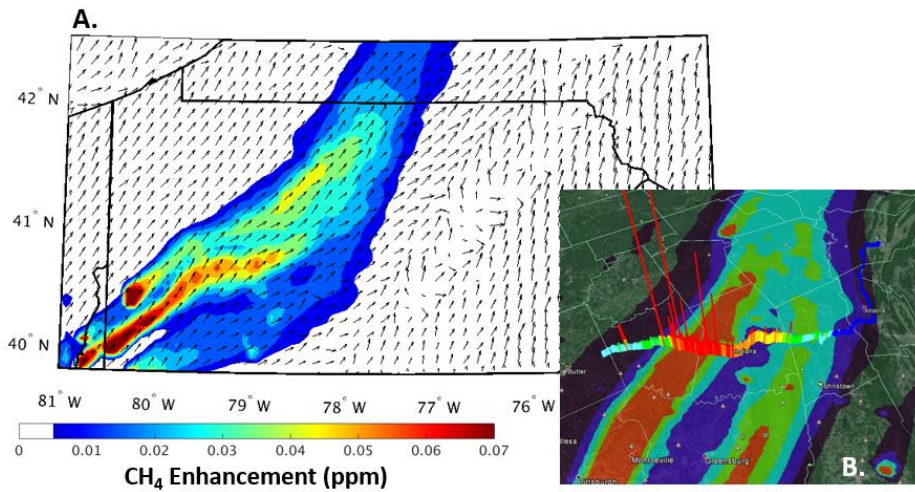


Figure 87: (a.) Model projected CH₄ enhancement at the surface associated with underground, surface, and abandoned coal mines on May 27th, 2015 at 19Z, with the shaded regions showing the CH₄ enhancement and the arrows representing the wind direction. (b.) Projected enhancement from a. mapped over measured CH₄ enhancement from a driving campaign. The height and colour of the bars represents the scale of the CH₄ enhancement.

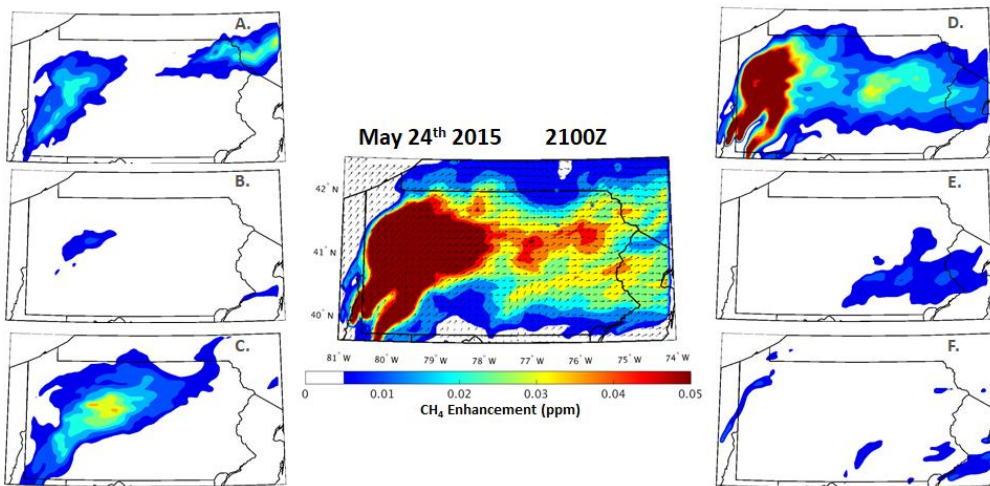


Figure 98: Projected CH₄ enhancements during the late afternoon flight of May 24th, 2015 at 2100Z, 700m above ground level from (A) upstream unconventional gas processes (B) downstream unconventional gas processes (C) conventional production (D) coal mines (E) animal emissions and (F) landfills and other sources within the EPA GHG Inventory Report. The centre figure is a map of the combined enhancement from sources A-F.

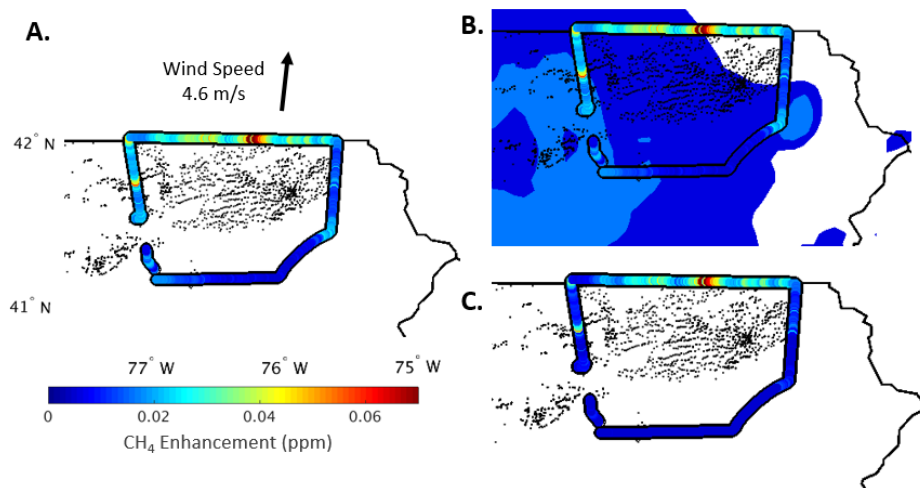


Figure 109: (a.) Observed CH₄ enhancements from within the boundary layer during the first loop of the May 29th aircraft campaign. (b.) Aircraft observations laid overtop modelled CH₄ concentrations at 700 m from sources unrelated to emissions from upstream gas production. (c.) Observed CH₄ enhancements from the May 29th flight after subtracting off modelled sources in b. The new set of observations represent the observation-derived upstream gas enhancement during the flight.

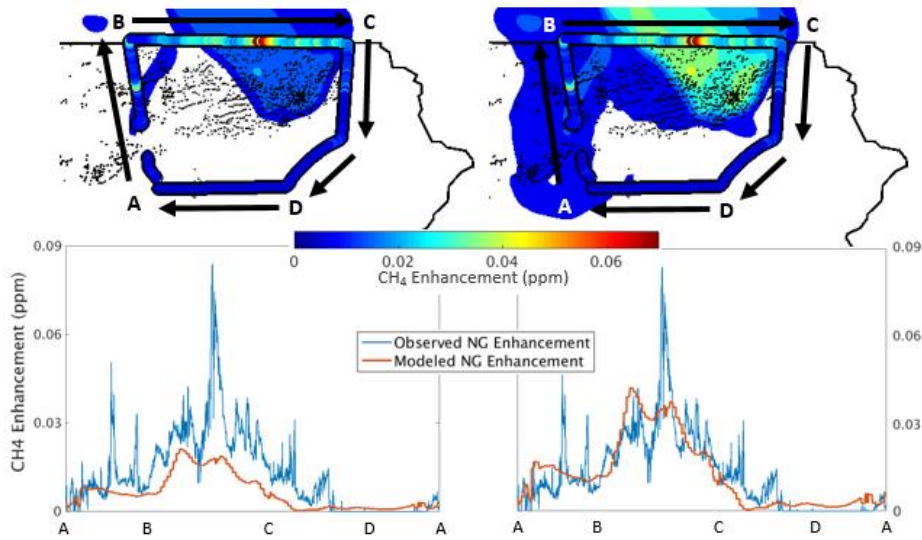


Figure 1110: (top-left) Observed enhancement from unconventional natural gas production overtop projected upstream natural gas enhancements at 700 m from the first loop of the May 29th flight, using an upstream gas emission rate of 0.13% of production. (bottom-left) Direct comparison of the observed natural gas enhancement vs. the modelled enhancement following the path from A-D using an unconventional emission rate of 0.13%. (top-right, bottom-right). Same as left figures, except using the optimized upstream emission rate of 0.26%

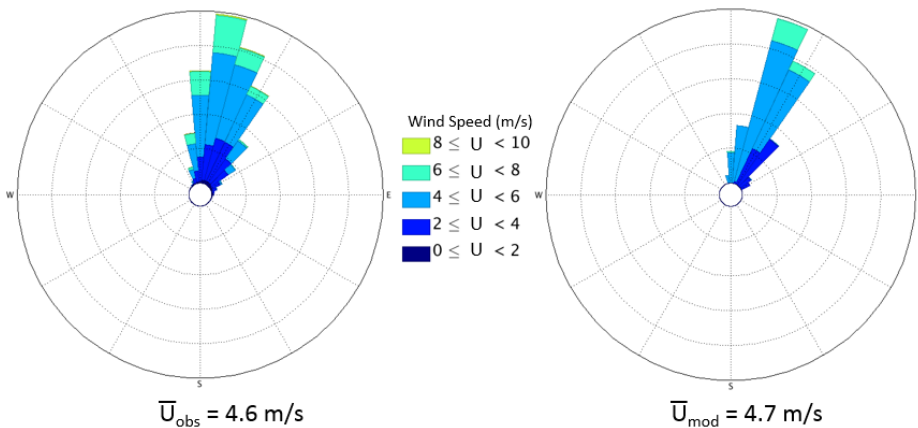


Figure 1211: Wind rose of aircraft observations (left) within the boundary from the first loop of the May 29th flight compared to modelled winds following the flight path (right).

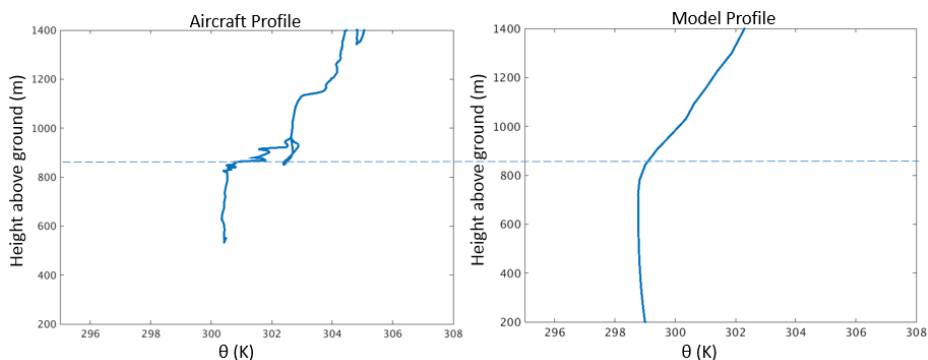


Figure 4312: (left) Observed potential temperature profile with height from the first aircraft spiral on the May 29th flight at 17Z. (right) Modelled potential temperature at the location and time at which the aircraft spiral occurred. In both cases, an inversion in the potential temperature profile begins to occur around 850m.

May 24th 2015: Late-Afternoon Flight

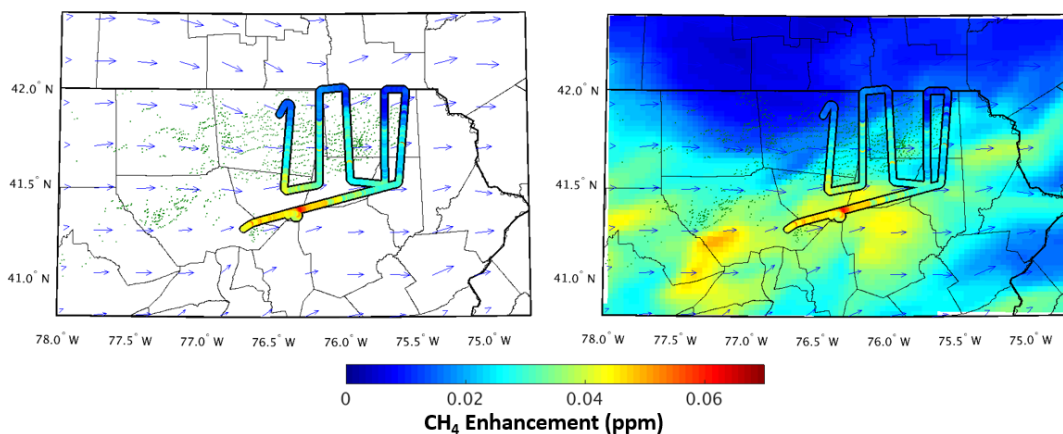


Figure 4413: (left) Observed CH₄ enhancement from the late-afternoon flight on May 24th, 2015. (right) Observed CH₄ enhancement compared to the model projected CH₄ enhancement from the sum of all sources in the region. The colour scale of observed and projected enhancements is scaled 1:1, with matching colours indicating matching values. Modelled wind vectors and CH₄ concentrations are from 700 m model height level.

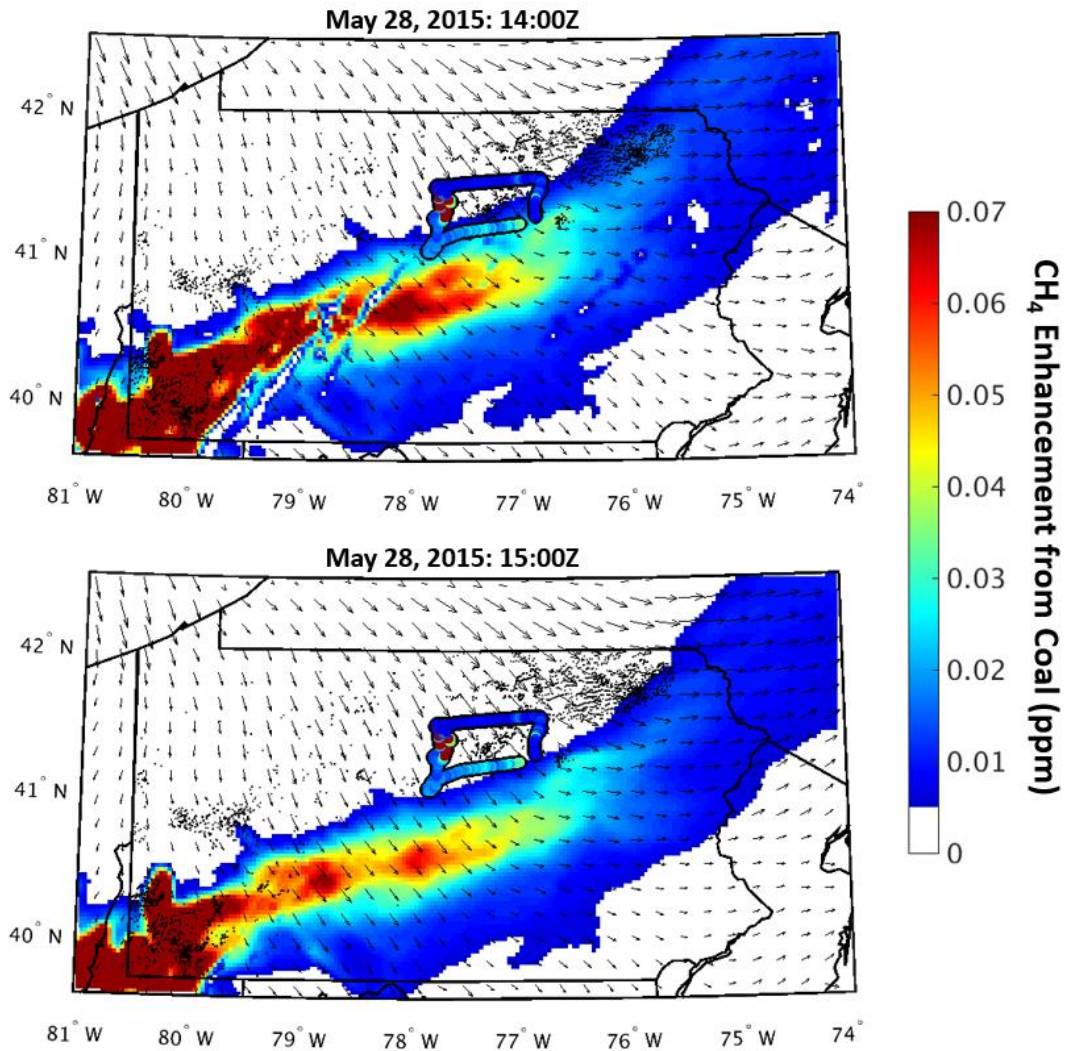


Figure 1514: Observed CH₄ enhancements from an early flight on May 28th, 2015 compared to projected CH₄ enhancements from coal emissions modelled at (top) 14:00Z and (bottom) 15:00Z. The one hour time difference results in vastly different projected enhancements across the southern portion of observations. Modelled wind vectors and CH₄ concentrations are from the 700 m model height level.

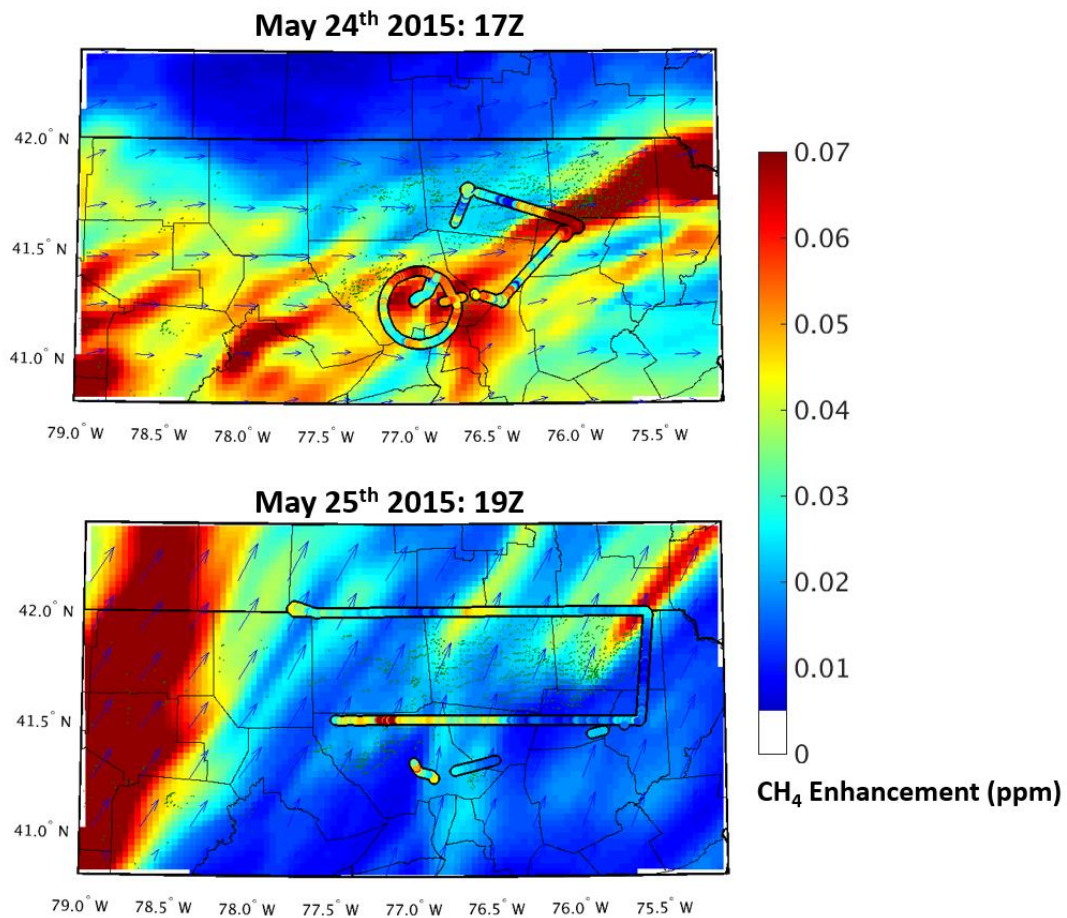


Figure 4615: Observed vs model projected CH₄ enhancements during (top) the early afternoon flight of May 24th, 2015 at 17Z and (bottom) the flight of May 25th, 2016 at 19Z. Modelled wind vectors and CH₄ concentrations are from 700 m model height level.

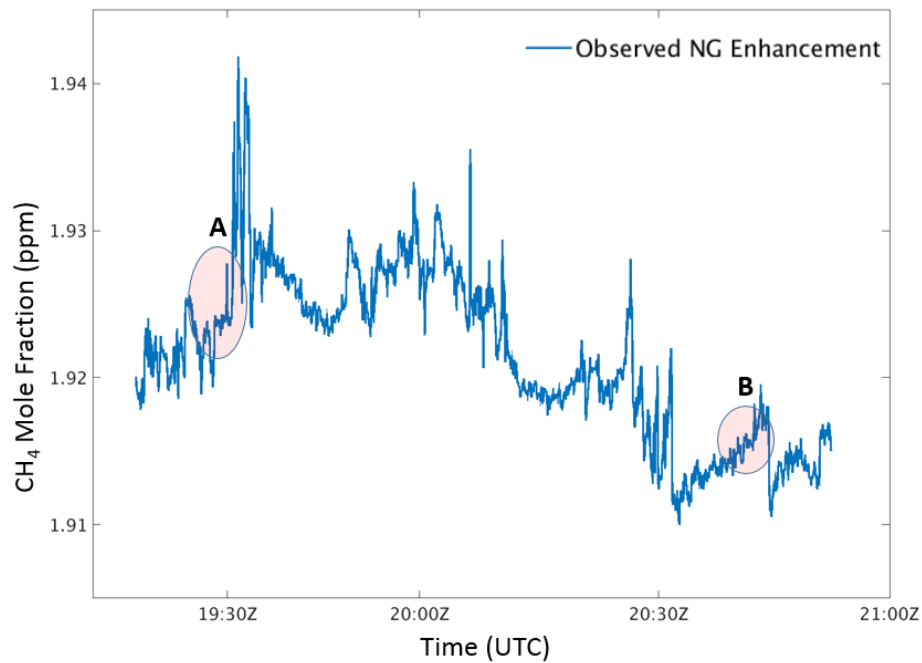


Figure 4716: Time series of CH₄ mole fractions from the second loop of the May 22nd flight. Observations at the shaded areas below A and B were taken at similar locations in space, showing the change in the background mole fraction across time.

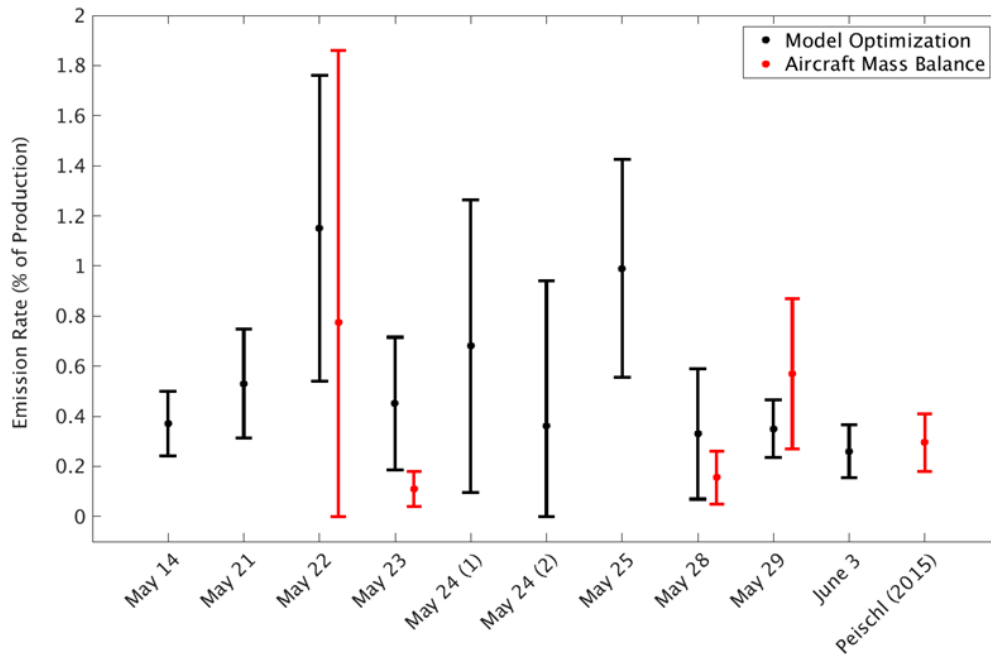


Figure 4817: Calculated upstream natural gas emission rates using (black) model optimization technique and (red) aircraft mass balance technique. Error bars represent the 2σ confidence interval for each flight. Mass balance performed in Peischl et al (2015) included for comparison.

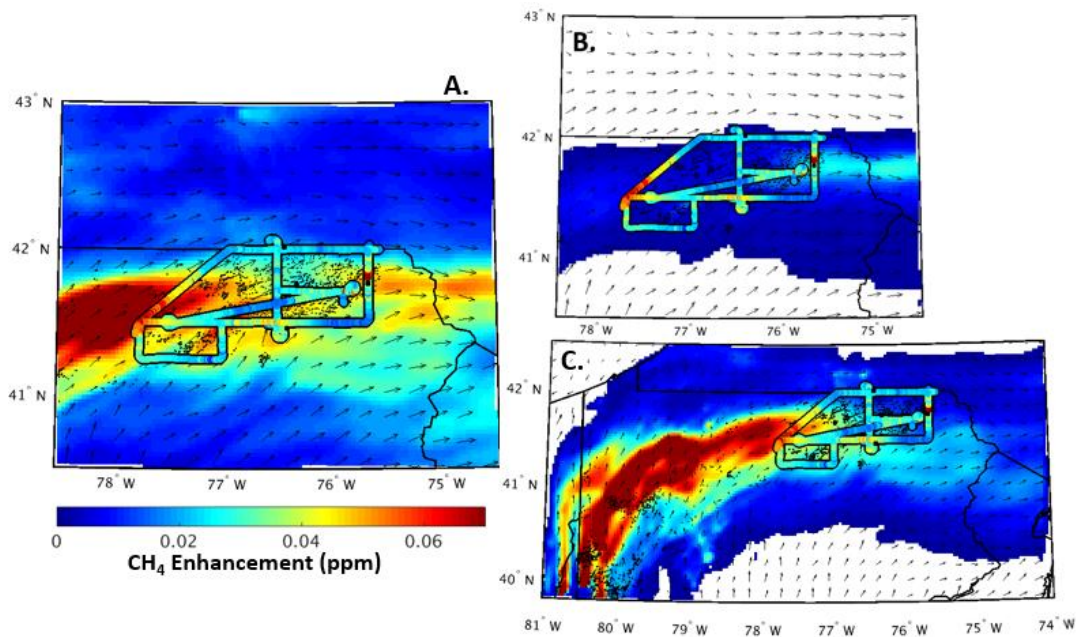


Figure 1918: Observations vs modelled enhancements of the flight from Peischl et. al (2015) for July 6th, 2013. (a.) Observed enhancements from the flight over model projected enhancements from all sources at 21Z. (b.) Projected enhancement from upstream gas processes using a 0.4% emission rate. (c.) Projected enhancement from coal sources in southwestern PA. Modelled wind vectors and CH₄ concentrations are from 700 m model height level.

Formatted: Caption, Indent: Left: 0", First line: 0"